AFRL-RH-WP-TR-2020-0014

MECHANISTIC INTERPRETATION OF HYPOBARIA AND HYPEROXIA USING OMIC TECHNOLOGY

Matthew W. Grogg, Sarah T. Pfahler, Meghan K. Makley, Molly E. Chapleau
Latha Narayanan, April Daubenspeck, Molly K. Miklasevich

Henry M. Jackson Foundation

Joyce G. Rohan

Naval Medical Research Unit Dayton

Andy Neufelt, Nicholas V. Reo

Wright State University
Department of Biochemistry and Molecular Biology

Michael C. Moulton, Lt. Correy R. Vigil, David R. Mattie, Deirdre A. Mahle

Airman Bioengineering Division
Applied Biotechnology Branch

MARCH 2020
Final Report

AIR FORCE RESEARCH LABORATORY
711TH HUMAN PERFORMANCE WING,
AIRMAN SYSTEMS DIRECTORATE,
WRIGHT-PATTERSON AIR FORCE BASE, OH 45433
AIR FORCE MATERIEL COMMAND
UNITED STATES AIR FORCE

NOTICE AND SIGNATURE PAGE

Using Government drawings, specifications, or other data included in this document for any purpose other than Government procurement does not in any way obligate the U.S. Government. The fact that the Government formulated or supplied the drawings, specifications, or other data does not license the holder or any other person or corporation; or convey any rights or permission to manufacture, use, or sell any patented invention that may relate to them.

Qualified requestors may obtain copies of this report from the Defense Technical Information Center (DTIC) (http://www.dtic.mil).

AFRL-RH-WP-TR-2020-0014 HAS BEEN REVIEWED AND IS APPROVED FOR PUBLICATION IN ACCORDANCE WITH ASSIGNED DISTRIBUTION STATEMENT.

//signature//

DAVID R. MATTIE, Work Unit Manager
Applied Biotechnology Branch
Airman Bioengineering Division

//signature//

RICHARD D. SIMPSON, DR-IV, DAF
Chief, Airman Bioengineering Division
Airman Systems Directorate
711thHuman Performance Wing
Air Force Research Laboratory

This report is published in the interest of scientific and technical information exchange and its publication does not constitute the Government's approval or disapproval of its ideas or findings.

REPORT DOCUMENTATION PAGE

Form Approved
OMB No. 0704-0188

1. REPORT DATE *(DD-MM-YY)*	2. REPORT TYPE	3. DATES COVERED *(From - To)*
	Final Report	October 2012 – February 2020

4. TITLE AND SUBTITLE
Mechanistic Interpretation of Hypobaria and Hyperoxia Using Omic Technology

5a. CONTRACT NUMBER
In-House

5b. GRANT NUMBER

5c. PROGRAM ELEMENT NUMBER
00000F

6. AUTHOR(S)
Matthew W. Grogg[1], Sarah T. Pfahler[1], Meghan K. Makley[1], Molly E. Chapleau[1], Latha Narayanan[1], April Daubenspeck[1], Molly K. Miklasevich[1,2], Joyce G. Rohan[2], Cary Honnold[2], Andy Neufelt[3], Nicholas V. Reo[3], Michael C. Moulton[4], Correy R. Vigil[4], David R. Mattie[4], Deirdre A. Mahle[4]

5d. PROJECT NUMBER
7757

5e. TASK NUMBER
HD

5f. WORK UNIT NUMBER
H0D1 (7757HD05)

7. PERFORMING ORGANIZATION NAME(S) AND ADDRESS(ES)
[1]HJF, 2728 Q St, Bldg 837, WPAFB OH 45433
[2]NAMRU D, 2728 Q St, Bldg 837, WPAFB OH 45433
[3]Wright State University, Biochemistry and Molecular Biology Dept., Dayton OH

8. PERFORMING ORGANIZATION REPORT NUMBER

9. SPONSORING/MONITORING AGENCY NAME(S) AND ADDRESS(ES)
[4]Air Force Materiel Command
Air Force Research Laboratory
711th Human Performance Wing
Airman Systems Directorate
Airman Bioengineering Division
Applied Biotechnology Branch
Wright-Patterson AFB, OH 45433

10. SPONSORING/MONITORING AGENCY ACRONYM(S)
711 HPW/RHBB

11. SPONSORING/MONITORING AGENCY REPORT NUMBER(S)
AFRL-RH-WP-TR-2020-0014

12. DISTRIBUTION/AVAILABILITY STATEMENT
Distribution A: Approved for public release. MSC/PA-2020-0072 88ABW-2020-1154, cleared 25 March 2020

13. SUPPLEMENTARY NOTES
Report contains color

14. ABSTRACT

Sprague-Dawley (SD) rats were exposed to pressures correlating to ambient (CTL; 21% O2, 1000 ft) or hyperoxic only (HYP; 100 % O2, 1000 ft) or high altitude plus hyperoxic (ALT; 100% O2, 30,000 ft above sea level) for 6-8 hours. Exposures were repeated 8-10 times over a 2 week period. Proteomic techniques showed that exposure to HYP or ALT for these durations resulted in distinct protein profiles for significantly regulated proteins with trends for pathway regulation in hippocampus and cortex. NMR-based metabolomics indicated exposing rats to hypobaria and/or hyperoxia had no effects on brain lipid metabolite profiles measured in cerebellum or cortex. Hyperoxia did not increase corticosterone in serum while in ALT there was a significant increase compared to control rats. No differences in glutathione were observed in brain or lung tissue between exposure groups and controls. Levels of malondialdehyde (MDA) were significantly higher in cortex of HYP compared to controls. In brainstem for ALT, levels of MDA decreased significantly relative to control and differed significantly between AL and HYP. Electrophysiology suggested repeated prolonged exposures to 100% oxygen results in hyper-excitability of hippocampal neurons. No changes were seen by histopathological examination of brains from exposed rats.

15. SUBJECT TERMS

U-2, Sprague-Dawley rats, hypobaria, hyperoxia, proteomics, nuclear magnetic resonance, oxidative stress

16. SECURITY CLASSIFICATION OF:			17. LIMITATION OF ABSTRACT:	18. NUMBER OF PAGES	19a. NAME OF RESPONSIBLE PERSON (Monitor)
a. REPORT	b. ABSTRACT	c. THIS PAGE			David R Mattie
Unclassified	Unclassified	Unclassified	SAR	57	19b. TELEPHONE NUMBER *(Include Area Code)* N/A

TABLE OF CONTENTS

Contents

LIST OF FIGURES

LIST OF TABLES

PREFACE

Funding for this project was provided through the Defense Health Program and the Aerospace Toxicology Program, which was part of the Aerospace Physiology and Toxicology Program in the 711 Human Performance Wing of the Air Force Research Laboratory. This research was conducted under cooperative agreement FA8650-15-2-6608 with the Henry M. Jackson Foundation for the Advancement of Military Medicine (HJF). The program managers for the HJF cooperative agreement were David R. Mattie, PhD and Armando Soto (711 HPW/RHB formerly RHXJ). David R. Mattie, PhD was also the program manager for this project.

The protocol "Mechanistic Interpretation of Hypobaria and Hyperoxia Using Omic Technology in a Sprague Dawley Rat (*Rattus norvegicus*)" was approved by the Wright-Patterson AFB Installation Animal Care and Use Committee (IACUC) as protocol number F-WA-2018-0170-A. The study was conducted in a facility accredited by the Association for the Assessment and Accreditation of Laboratory Animal Care (AAALAC) International, in accordance with the Guide for the Care and Use of Laboratory Animals (NRC, 2011). The study was performed in compliance with DODI 3216.1.

The authors would like to acknowledge the US Army Medical Research Institute of Chemical Defense for preparing the slides of brain tissue for Col Honnold. The slides were stained for H&E and Luxol Fast Blue.

1.0 SUMMARY

The U-2 is a specialized plane that flies at altitudes much higher than fighter jets and commercial airplanes. Because of this high altitude, pilots of U-2 aircraft breathe 100% oxygen before and during the flight to provide enough oxygen and to prevent any illness associated with the altitude. However, long flights at high altitude and breathing high concentrations of oxygen appear to have adverse health effects. Medical imaging of U-2 pilots has shown spots in the brain that typically only appear in aged brains. The abnormal brain images from U-2 pilots may indicate a loss of brain tissue or scarring. These changes were not seen in Air Force non-flying personnel (altitude chamber technicians are an exception). A decrease in cognitive abilities has also been shown to occur in pilots with abnormal imaging and is linked to these changes (McGuire et al., 2014). A pilot study has been completed that established the ability to expose rats to high altitude and high oxygen. Neuronal and lung tissues exhibited metabolomics, gene expression, and proteomic changes, despite the mild nature of the exposures (AFRL-RH-WP-TR-2018-0001). Several of these changes were seen in rats with the highest levels of corticosterone which was measured in the serum of rats. This follow-on study further investigated these effects with more intense exposures of high altitude and high percentage of oxygen, using a Sprague-Dawley (SD) rat model. Rats were exposed to pressures that correlated to ambient/control (CTL; 21% O2, 1000 ft) or hyperoxic (HYP; 100 % O2, 2500 ft) or high altitude (ALT; 100% O2, 30,000 ft above sea level) for 6-8 hours. The exposures were repeated 8-10 times over a 2 week period.

This rodent study was an integrated effort of multiple disciplines that will contribute to a mechanistic understanding of the effects of extreme hypobaria and hyperoxia. Proteomic techniques were used to identify major up and down-regulated proteins in brain which were then correlated to biological pathways and cellular functions to highlight key regions of disrupted or modified pathways or cellular functions that were affected. Nuclear magnetic resonance (NMR)-based metabolomics was performed to determine the perturbation of brain lipid profiles, changes in which might be tied to any histological damage or change. Because extreme hypobaria and 100% oxygen are unique stressors, biochemical assays were used to measure general stress, oxidative stress and inflammation. Proteomic techniques were used to identify major up and down-regulated proteins in the brain which were then correlated to biological pathways and cellular functions. Exposure to HYP or ALT for longer durations resulted in distinct protein profiles for significantly regulated proteins showing trends for pathway regulation in the hippocampus and cortex. HYP exposure resulted in more protein changes than in the ALT group. Nuclear magnetic resonance (NMR)-based metabolomics indicated that exposing rats to hypobaria and/or hyperoxia appears to have no significant effects on brain lipid metabolite profiles measured in cerebellum or cortex.

Biochemical assays were conducted on brain tissue to measure oxidative stress (enzymatic antioxidants, lipid peroxidation) and corticosterone in blood for stress. Corticosterone measured in serum to quantify the level of generalized stress did not increase with hyperoxia while in the altitude group there was a significant increase compared to the control rats. Malondialdehyde (MDA) is a product of lipid peroxidation and is a marker of oxidative stress. MDA was assayed in all brain regions except hippocampus. In cerebellum, levels of MDA were no different in

either treatment group relative to control, yet variability was high. Levels of MDA were significantly higher in cortex from the hyperoxia group as compared to control. In brainstem, when rats were exposed to hypobaria (ALT), levels of MDA decrease significantly relative to control. In addition, MDA levels differed significantly between hypobaric (ALT) and hyperoxia (HYP). Glutathione exists in its reduced (GSH) and oxidized (GSSG) forms, and an increased GSSG-to-GSH ratio is indicative of oxidative stress; there were no differences observed in brain tissue or lung tissue between the exposure groups as compared to the control.

Electrophysiological changes were measured in hippocampus, using a multi-electrode array for stimulating and recording field potentials. Three parameters were measured: (1) neurotransmission; (2) spontaneous activity; (3) synaptic plasticity. The data suggest that repeated prolonged exposures to 100% oxygen can result in the hyper-excitability of hippocampal neurons. Complete histopathological examination of brain from exposed rats using both hematoxylin and eosin staining, as well as luxol fast blue for damage to myelination did not find any histologic changes.

The data from this study will be shared with researchers of a mini-pig study for joint interpretation. The potential payoff of the knowledge gained from these studies is a better approach to mitigating or preventing operational risks and long term adverse health outcomes associated with high altitude flight and operation of altitude chambers.

2.0 INTRODUCTION

High altitude U-2 pilots and altitude chamber technicians show increased incidence of leukoraiosis or white matter hyperintensities (WMH) in T2 weighted magnetic resonance imaging (MRI) of brain, indicative of hypodensities linked to neuronal loss, demyelination and gliotic scarring (McGuire et al., 2013; McGuire et al., 2012). Before 2012, pilots of U-2 aircraft flew in cabins pressurized to approximately 30,000 ft. Pilots also pre-breathe 100% O_2 for 1 h prior to flight and continue with 100% O_2 for the duration of the flight in order to remove nitrogen dissolved in the blood. It has been hypothesized that exposure to extreme hypobaria, excess oxygen, or a combination of both stressors, irrespective of decompression sickness, is the primary causative factor for these WMH. A one year pilot/exploratory study in rodents (project 15-036) was designed and completed to complement a concurrent minipig study that was performed at Lackland AFB by Col Paul Sherman, MD and Dr Stephen McGuire. The minipig study mimics the exposure scenario of a U-2 pilot with 100% O_2 and hypobaric pressures equivalent to 30,000 ft. The minipigs were exposed for long durations with multiple repeats. The intent of the minipig study was to induce the formation of WMH and use histopathological examination to determine the etiology of the lesions. The hypothesis of the rodent study was that the extreme stressors that a high altitude pilot experiences (hypobaria, 100% O_2) would cause perturbations in the normal signaling and biological processes of the brain that are early indicators of neuronal dysregulation and, potentially, lesions. The rodent study was an integrated effort of multiple disciplines to contribute to a mechanistic understanding of the effects of extreme hypobaria to the pathophysiological studies being conducted in mini-pigs. The preliminary rat study was successful in generating an altitude chamber system capable of the extreme conditions of hypobaric pressures equivalent to greater than 30,000 ft and delivering 100% O_2 safely and effectively to the rodents. Although the rats appeared to tolerate hypobaric pressures well, serum corticosterone data showed that both hyperoxic and hypobaric exposures were stressful to the animals. Pro-inflammatory markers (IL-6, IFN-γ and TNF-α) were increased in lung. IFN-γ was increased in heart after both hyperoxic and hypobaric exposure. Proteomic analysis of brainstem showed that both hyperoxic and hypobaric exposure caused changes in proteins associated with energy metabolism, axon guidance, gene expression, signal transduction, protein folding, adhesion, synaptic transmission and cell growth. Preliminary Principal Component Analysis (PCA) of cerebellum lipid data from nuclear magnetic resonance (NMR) spectra showed that there is complete separation of the altitude group from the control group, indicating significant differences in the spectral features.

The pilot study showed that protein and metabolite changes occurred after exposure to hypobaric and hyperoxic conditions with significantly more protein changes in the hyperoxic group. However, the rats appeared to be fairly tolerant of the exposure conditions, and, as a possible result, the effects seen from the pilot rodent study were minimal. Similar tolerance was seen with the minipig study (personal communication, Col Paul Sherman). As a result of this, a follow on study was funded to increase the intensity of the exposure conditions significantly and to replicate more closely the operational tempo of a U-2 pilot. In the original study, the total exposure time for each rat was 12 h. In this study, the exposure time was increased up to 60 h total. The duration of each daily exposure was increased from 4 h up to 7 h in a single day. The number of repeated exposures changed from 3 to 8 over the course of 2 weeks. Increasing the number of repeated exposures was a key component of this study. This experimental paradigm

created a scenario where the brain had to continually reestablish homeostasis, potentially leading to progressive and complex injury pathways that exceed the resiliency of cells. The treatment groups remained the same with the exception of increasing the hyperoxic group to 2500 feet of altitude (for animal safety reasons): control (CTL; 21% O_2, 1000 ft); hyperoxic (HYP; 100 % O_2, 2500 ft); altitude (ALT; 100% O_2, 30,000 ft). Because changes were seen under the original conditions, it was expected that the change in intensity will augment the effects previously observed, allowing for more definitive connections with the signaling pathways and biological functions/processes that are impacted. This would also then allow for a deeper understanding of the mechanistic basis of the adverse effects of high altitude flight-like conditions.

It is recognized that the rat brain is different in size, structure and vasculature from the human brain, and, therefore, not the perfect model for investigating the induction of WMH. Interestingly, it is known that WMH can be induced in a rat model after an ischemic event (Huang et al., 2010). The approximately 5X higher total exposure time for these proposed studies may result in increased neuronal dysregulation and, ultimately, lesions. Since imaging is not available, histopathological examination will be the only way to determine if structural changes have occurred. While not an exact model of the human brain, the individual cellular genetic and pathway response causing an altered phenotype to the stressors of hypobaria and hyperoxia are certain to be the same between species. Likewise, if there are regional differences in the effects of hypobaria or hyperoxia (hippocampus vs cerebellum), those changes should be quite similar, as well.

Proteomic techniques will again be used to identify major up and down-regulated proteins that will then be correlated to biological pathways and cellular functions. Nuclear magnetic resonance (NMR)-based metabolomics will be used to determine the perturbation in brain lipid profiles, which would provide key events associated with white matter changes and effects. Biochemical assays will also be used to measure general stress, oxidative stress and inflammation. Neuroelectrophysiology will be added in order to detect changes in neuronal function, especially those linked to cognitive functions. Histological examination of the brain sections will also be added to detect any functional or structural changes caused by extended exposure conditions.

3.0 METHODS

General methods that pertain to both studies are detailed in Sections 3.1 through 3.5. Specific methods for the acute and two-week studies are found in Sections 3.6 and 3.7, respectively. Method related excerpts from the approved animal use protocol can be found in Appendix A.

3.1 Altitude Chamber Set Up

The altitude system consists of a custom built 20”x20.5”x20” stainless steel chamber (Laco Technologies, Salt Lake City, UT) with 27 ports and a 1.5” thick acrylic door (Figure 1). The chamber can withstand hypobaric conditions to an equivalent altitude of 50,000 feet. The chamber pressure was monitored from three distributed ports using oxygen cleaned, intrinsically safe, pressure sensors from American Sensors Technology (AST, Mt Olive, NJ). A whole body exposure chamber was fitted within the altitude chamber to contain both the rats and the test atmosphere. The test atmosphere was generated using Teledyne mass flow controllers, supplied from compressed gas cylinders, and transported within stainless steel tubing with an inert coating. Immediately upon exiting the whole body chamber, the test atmosphere was mixed with nitrogen such that the vented atmosphere contained no more than 20% O_2. The simulated altitude was achieved and maintained by an Edwards 10iC vacuum pump with an inline Aalborg needle valve. Test atmosphere and simulated altitude were controlled via a computer interface with customizable programs created in LabVIEW (Austin, TX). For the purposes of this report the term altitude refers to the equivalent pressure.

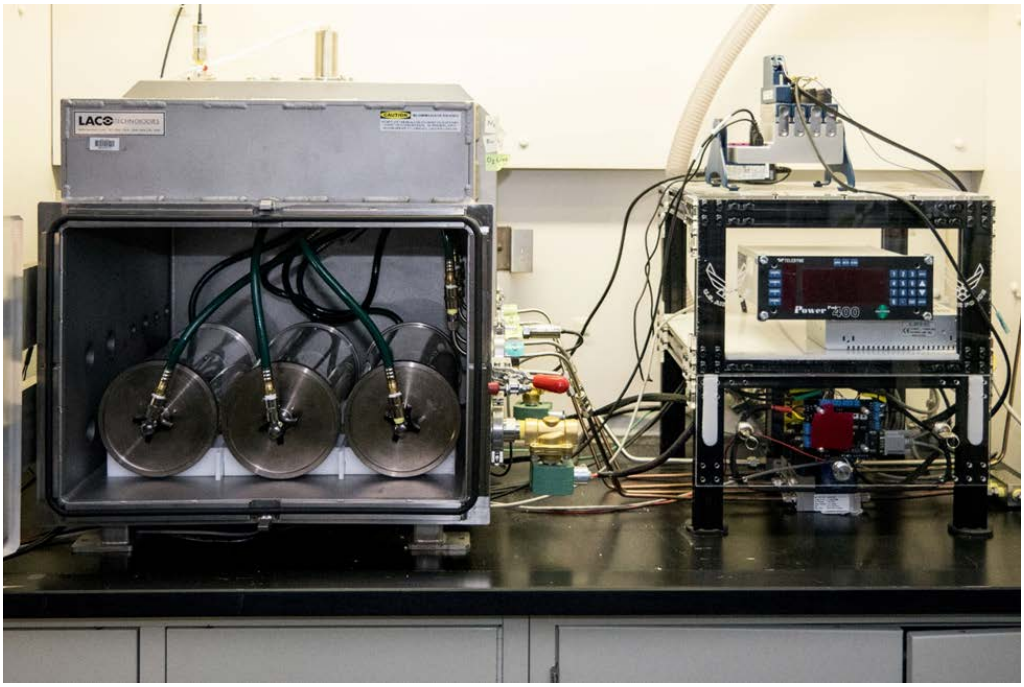

Figure 1. Altitude chamber system.

Stainless steel altitude chamber set up, including control tower (on right) with mass flow controllers. Within the altitude chamber (left) are 3 animal holding tubes, capable of housing two rats each. Entire system is computer controlled by custom software developed in LabVIEW System Design Software (National Instruments).

3.2 Exposure Scenario

Rats were divided into three exposure groups: CTL (ambient pressure, normoxic), ALT (30,000 feet, 100% oxygen) and HYP (2500 feet, 100% oxygen). The rats in the ALT group pre-breathed 100% O_2 for 10-30 min prior to flight. The ascent to 30,000 ft was 1000-2000 ft/min, requiring 15-30 min to ascend. Descent followed the same profile. The HYP group remained included in order to separate effects caused by oxygen toxicity versus those caused by hypobaria. It is important to note that at pressures equivalent to 30,000 ft, 100% O_2 may still cause an elevated piO2, but not high enough to be considered toxic. Both the CTL and HYP groups followed an ascend (and descend) protocol similar to the ALT group with the exception of the exposure altitude level, providing the same pump noise and vibration as the ALT group. Six rats were used for each treatment group. Based on the limited size of the brain regions and the preparation requirements (formalin fixation versus flash freezing), separate cohorts were used for proteomics/metabolomics, biochemical assays, pathology and electrophysiology (6 rats/group X 3 groups X 4 cohorts: Total # rats = 72; Table 1) Each of the 3 tubes within the altitude chamber contained 2 rats, and 6 rats were exposed at a time. Cage-mates were exposed together in the same exposure tube. Post exposure they were returned to their regular cage and housed together. The rats were able to move freely. Water was provided during the exposure in the form of hydrogels. Conditions were monitored continuously in real-time over the course of the exposure. A camera was installed for additional monitoring capabilities. The exposure tubes were cleaned in between every exposure using soap and water and then aired out overnight. The exposure time was from ~7 h/day and was repeated 8 times over the course of 2 weeks. Animals were housed socially with their cage-mate/exposure mate in between exposures. Animals were euthanized 5 min following the last exposure and blood, brain, lungs and heart were collected. It was previously determined that rats are tolerant to the exposure conditions; therefore, no tolerance testing was included.

3.3 Mass Spectrometry-based Proteomics

3.3.1. Mass Spectrometry-based Proteomics – Sample Preparation

Brain tissue (10 mg) was homogenized in a RINO tube containing lysis buffer consisting of 7 M urea, 2 M Thiourea, 100 mM triethylammonium bicarbonate (TEAB), and 500 µL MS-SAFE Protease and Phosphatase Inhibitor (Sigma-Aldrich). After discarding the pellet, beads, and separated layer, the proteins were reduced with 5 µL dithiothreitol (DTT) to a final concentration of 5 mM for 60 min at 37°C. After the samples had cooled to room temperature, they were alkylated with 15 µL iodoacetamide to a final concentration of 15 mM for 20 min in the dark followed by dilution with 600 µL of 50 mM Tris-HCl (pH 8) to achieve a $\leq$ 1 M urea concentration. Each lysate was quantified using the BCA protein assay kit (Thermo Fisher) according to the manufacturer instructions. Samples were then normalized to 100 µg/ 100 µL. Proteins were digested overnight at 37°C using 3 µg sequencing-grade modified Lys-C/Trypsin (Promega). The reaction was halted with 10 µL of 10% trifluoroacetic acid (TFA) for a final concentration of 1%. Samples were centrifuged at 14,000 x g for 10 minutes. Tryptic digests were evaporated by a vacuum concentrator, and then resuspended in a volume of 100 µL of 0.1% TFA in water. Any air bubbles were ruptured with IPA gas. Peptides were desalted using C18 peptide cartridges and evaporated down to a volume of 20 µL by a vacuum concentrator, and then brought to a final concentration of 0.50 µg/µL.

3.3.2. Mass Spectrometry-based Proteomics – Analysis

A total of 38 samples (and two pooled samples) per treatment group were analyzed using a Thermo Fusion Lumos LC system coupled with a Q Exactive HF mass spectrometer (Thermo Fisher). Samples were run at a flow rate of 300 nl/min at 37°C. Peptides were eluted with a step-wise gradient of solvent A: 0.1% formic acid in water versus solvent B: 0.1% formic acid in acetonitrile starting at 3% solvent B for 7.5 min, 30% solvent B at 117 min, 40% solvent B at 122 min, 90% solvent B at 127 min, 3% solvent B at 140 min for 10 min. The eluent was ionized using an uncoated capillary tip in a Thermo spray source operating in positive ion mode. Mass spectra were acquired in data dependent mode, switching automatically between MS and MS/MS acquisition. All full-scan MS spectra in the range from *m/z* 400 to 2000 were acquired at a resolution of 60000 in the FT-MS. The AGC target was 3,000,000 with an injection time of 20 ms. The 5 most intense ions from each scan were selected for MS/MS analysis using CID. The MS/MS spectra range was 200 to 2000 *m/z* with a resolution of 15,000. The MS/MS AGC target setting was 100,000 and ion injection time was set to 25 ms.

3.3.3. Mass Spectrometry-based Proteomics – Data Analysis

The processing of the individual raw MS data files was conducted using a rat protein database in MaxQuant 1.6.5.0 with its integrated search engine Andromeda and target decoy database with a false discovery rate cutoff of 1%. Protein intensities were calculated using the algorithms developed for labeled-based quantification by Tyanova et al. 2016. Methionine oxidation and cysteine carbamidomethylation were included in the database search. Protein intensities were calculated as sum of reporter intensities multiplied by injection time for each isobaric labeling channel for all MS/MS spectra matching to the protein group if a minimum of two peptides were identified of which at least one had to be unique. If a peptide were identified as shared between two proteins (razor peptide), it was used for quantification of the protein group with a larger number of associated proteins or, in the case of a tie, to the protein group with higher-scoring peptides in the Andromeda search. Protein fold changes of individual protein intensities were calculated by using the average of pooled protein intensities of the CTL samples as the denominator. Proteins were identified as regulated if the corresponding p values were less than 0.05, based on the one-sample Student t-test, and if the absolute $\log_2$ fold-change was more than 0.58. The data were further analyzed through functional interaction network software (Qiagen's Ingenuity Pathway Analysis) to understand and visualize the protein pathways that were modulated by hypobaria or excess oxygen. Secondary computational analysis was executed using Perseus 1.6.0.2 (Tyanova et al. 2016b) for statistical rendering.

3.4 NMR-based Metabolomics

3.4.1. NMR-based Metabolomics – Sample Preparation

Each brain region was extracted by a modified version of the dual phase method of Tyagi et al. (1996). Briefly, the frozen powder was quickly transferred to a tared 20 mL glass homogenizer tube, and the weight recorded. Ice cold methanol (MeOH) was immediately added to the tube at 0.7 mL/100 mg tissue, and the mixture was homogenized on ice with a chilled Teflon pestle at 20 rpm (in reverse mode). The homogenate was allowed to stand on ice for 15 min. Chilled chloroform ($CHCl_3$) at 0.7 mL/100 mg tissue was added, and the mixture was homogenized at 20 rpm. Chilled double distilled water (ddH_2O) was added at 0.7 mL/100 mg tissue, and the

mixture was homogenized at 20 rpm. The mixture was transferred to an ice cold 50 mL glass centrifuge tube and allowed to stand on ice for 15 min before centrifuging at 2000 x g for 25 min at 4°C. In the meantime, a separatory flask and funnel were placed in a refrigerator at 4°C. A #1 filter paper disc was placed in the funnel and primed with 0.5 mL each of MeOH, $CHCl_3$ and ddH_2O, in that order. The supernatant was transferred to the flask. The homogenizer tube was washed with 0.5 mL each of MeOH, $CHCl_3$ and ddH_2O and the mixture was re-homogenized. The wash was allowed to stand on ice for 5 min, then transferred to the same centrifuge tube and centrifuged at 2000 x g for 5 min at 4°C. The supernatant was then added to the separatory funnel. This procedure was repeated three more times. After the supernatant was completely filtered, the mixture was allowed to stand at 4°C for 17-24 hr to allow complete separation of the two liquid phases.

Once separation was complete, the separatory flask was moved to room temperature and allowed to sit for 2 hr. The upper aqueous phase was carefully aspirated with a disposable pipet and transferred to a 60 mL lyophilizer flask. The lower organic phase was drained into a pre-weighed 10 mL amber vial. The separatory flask was washed 3 times with 0.5 mL each of ddH_2O, MeOH, and $CHCl_3$, allowing the solution to sit for 45 min between each wash for complete phase separation. Aqueous and organic phases were removed each time as before and added to the same vials from the first separation.

Lipid fraction. The amber vial containing the organic extract was placed in a 25°C water bath, and a gentle stream of nitrogen gas was blown over the top of the vial to evaporate the $CHCl_3$. The vial was then sealed with a black Viton septum (Fisher Scientific) and placed on vacuum overnight and then weighed. The dried lipid sample was reconstituted in 600 µL of 99.8% deuterated chloroform ($CDCl_3$). If the lipid weight was greater than 30 mg, then enough $CDCl_3$ was added to yield a lipid concentration of 50 mg/ml. The vial was crimp-sealed and stored at -20°C until analysis.

Aqueous fraction. The lyophilizer flask containing the aqueous extract was placed in a 25°C water bath and a gentle stream of nitrogen gas was blown over the top of the sample to evaporate the MeOH. After most of the MeOH was evaporated the lyophilizer flask was placed in liquid nitrogen to freeze the aqueous extract and then lyophilized to dryness overnight. The dried aqueous sample was reconstituted in 2 mL of ddH_2O, and 5 g/100 mL of Chelex 100 was added to remove divalent ions. The mixture was stirred at 4°C for 1 hr, then transferred to a 15 mL disposable centrifuge tube and centrifuged at 2000 x g for 10 min at 4°C to remove the Chelex. The supernatant was transferred to the original vial, with another 5 g/100 mL of fresh Chelex 100. The mixture was stirred again, at 4°C for 1 hr, transferred to the same 15 mL disposable centrifuge tube and centrifuged at 2000 x g for 10 min at 4°C. The supernatant was transferred to a pre-weighed 20 mL clear serum vial and covered with filter paper. The lyophilizer flask was rinsed 3 times with 2 mL of ddH_2O, transferring each washing to the same centrifuge tube. The tube was centrifuged at 2000 x g for 5 min at 4°C, transferring the supernatant to the same vial each time. The vial was placed in liquid nitrogen to freeze the aqueous extract and placed on a lyophilizer overnight. Once dry, the aqueous extract was weighed, crimp-sealed and stored at -20°C for subsequent NMR analysis.

Preparation of samples for NMR analyses. The dried aqueous extracts were reconstituted in 750 µL of 1.04 mM 2, 2`, 3, 3`-deuterotrimethylsilylpropionic acid (TSP) solution prepared in 99.99% deuterium oxide (D_2O). TSP was added as a chemical shift reference (set at 0.0 ppm) and internal standard for metabolite quantification (^{1}H NMR). For ^{1}H analysis, 650 µL of the reconstituted solution were added to a 5 mm NMR tube. For NMR analysis, lipid extracts were prepared in a three-part solvent system consisting of $CDCl_3$, MeOH and 90 mM aqueous Cs_2(EDTA) (Meneses and Glonck, 1988). The final lipid sample composition was 12:4:1 $CDCl_3$:MeOH:H_2O (v/v/v). Samples were placed into 5 mm NMR tubes and a ^{13}C NMR spectrum was acquired first, then triphenylphosphate (TPP) was added to the sample (50µL of 38 mM TPP in $CDCl_3$) and a ^{31}P NMR spectrum was acquired. TPP provided an internal standard for metabolite quantification. The sample volume was calculated by measuring the height of the lower phase, applying the formula for the volume of a cylinder and correcting for the curvature of the tube bottom.

3.4.2. NMR-based Metabolomics - Analysis

All NMR analyses were performed using a Varian INOVA 600 MHz spectrometer (14.1 T). High-resolution ^{1}H and proton-decoupled ^{31}P and ^{13}C NMR spectra of brain region extracts were acquired in field-lock mode using a 5 mm broadband probe operating at 600, 242 and 150 MHz, respectively. The sample temperatures were maintained at 20°C for lipid extracts to optimize spectral resolution (and minimize evaporation) and 25°C for aqueous extracts. Data acquisition parameters for ^{1}H included 8000 Hz spectral bandwidth, 4 s acquisition time, 6 s interpulse delay and 1.5 hr of signal averaging. C-13 parameters included a 70° pulse, 36 kHz spectral bandwidth and 4 s acquisition time, interpulse delay of 4 s, using a waltz ^{1}H-decoupling sequence with nuclear Overhauser enhancement (NOE) and approximately 20 hr of signal averaging. ^{31}P lipid data were acquired with ^{1}H decoupling and NOE using a 90° pulse, 7 kHz bandwidth, 1.9 s acquisition time, 3.9 s interpulse delay and approximately 18 hr of signal averaging.

3.4.3. NMR-based Metabolomics - Data Analysis

Using a Sun Microsystems computer and VNMR v6.1 software, NMR data were processed using exponential multiplication (0.3 Hz line-broadening for ^{1}H and 1 Hz for ^{31}P and ^{13}C spectra), Fourier transformation, manual phasing and baseline correction (5^{th} order polynomial and spline correction). The ^{1}H and ^{13}C NMR spectra were adaptively binned using a dynamic programming technique in MATLAB® (MathWorks, Inc., R2011b) that sets the minimum distance between peaks to 0.002 ppm and the maximum distance between peaks in a bin to 0.04 ppm (Anderson *et al*., 2010). The less complex ^{31}P spectra from lipid extracts were analyzed using a Gaussian-Lorentzian peak-fitting algorithm available in the VNMR software, which directly outputs peak areas that were used for metabolite quantification.

NMR chemical shift assignments for lipid resonances in the ^{13}C spectrum were taken from the literature (Forgacs *et al*. (2012), Halliday *et al*. (1988), Sillerud *et al*. (1986) and others). The $CDCl_3$ signal was set at 77.79 ppm for reference (relative to TMS at 0.0 ppm) and was used as the internal standard for quantification. ^{1}H NMR spectra of aqueous extracts and ^{13}C NMR spectra of lipid extracts were analyzed using multivariate data analysis tools, including Principal Component Analysis (PCA) and Orthogonal Projections onto Latent Surfaces Discriminant Analysis (OPLS-DA). Phosphorous NMR of lipid extracts were quantified using peak area after correcting for T_1 saturation and NOE. This correction was accomplished by acquiring a

reference spectrum from a representative sample under conditions of full relaxation with no NOE.

As a first approach PCA and OPLS-DA were used to examine whether treatments influenced metabolite profiles of aqueous brain extracts (^{1}H) and lipid extracts (^{13}C). The ^{13}C spectra can be examined in greater detail by measuring relative changes in various lipid metabolites such as cholesterol, triacylglycerol and some classes of fatty acids (FA) such as n3-FA and n6-FA. The C18, C19 and C14 carbons of cholesterol at 12.5, 19.7 and 57.2 ppm, respectively, were averaged for quantification. The signal in the range of 20.9 – 21.03 ppm represented the n2 carbon from all n3-FA, and the signal within the range of 32.03 – 32.29 ppm represented the n3 carbon of the n6-FA. These carbon signals shift slightly within this range because of the differences in carbon chain lengths of these fatty acids. The terminal methyl carbon of fatty acids at 14.8 ppm was used as a measure of the total FA pool. The signal at 27.3 ppm represented the polyunsaturated fatty acids (PUFA), specifically diallylic carbons, C=C-$\underline{C}H_2$-C=C. While this signal was integrated for a relative quantitative value of PUFA, it is important to note that its intensity is dependent upon both concentration and composition, and, therefore, is not an accurate measure of concentration.

For quantification purposes the ^{1}H, ^{31}P and ^{13}C NMR signal intensities were corrected for T_1 saturation and NOE, when necessary. To correct for T_1 saturation and NOE data were acquired for a representative cortex and brainstem sample under fully relaxed conditions ($5T_1$ with no NOE; interpulse delay of 250 sec for ^{13}C and 59 sec for ^{1}H). The ratio of the intensity of each signal selected to the $CDCl_3$ or TSP intensity was calculated for both fully relaxed (R_{FR}) and partially saturated (R_{PS}) spectra. Calculation of the R_{FR}/R_{PS} ratio provided the saturation factor for each signal of interest. For all analyses metabolite concentrations were normalized to tissue weight.

3.5 Assessment of Stress and Inflammation

3.5.1. Corticosterone Radioimmunoassay - Sample Preparation and Analysis

Assays for corticosterone in rat serum were performed using Immuchem Double Antibody Corticosterone ^{125}I RIA Kit (MP Biomedicals, LLC, Orangeburg, NY). Because serum was collected from all rats regardless of endpoint, the n for corticosterone was 12 not 6. Serum samples were prepared according to manufacturer's standard procedure by diluting 200 times with steroid diluent A. Rat tissue samples were diluted either 200 times or less with diluent A in order to obtain more sensitivity for the detection of corticosterone levels in tissue. The diluted samples were vortexed briefly prior to use. Samples and standards were run in duplicate. Assay kits from the same batch number and with the same expiration date were used for all corticosterone measurements.

3.5.2. Malondialdehyde - Sample Preparation and Analysis

Approximately 10 mg of each tissue homogenate was lysed via sonication for 15-20 seconds on ice in 303 µL of Lysis Solution. Lysates were centrifuged for 10 minutes at 13,000 x g and supernatants collected. A portion of the supernatant was reserved and used for protein determination (Pierce BCA Protein Assay Kit, Rockford IL). MDA-TBA (thiobarbituric acid)

adduct was generated as described in the manufacturer's protocol (Lipid Peroxidation MDA Assay Kit, Abcam, Cambridge MA). The MDA assay procedure was performed in a 95°C bead bath for 60 minutes. Tubes were moved to an ice bath for 10 minutes, then centrifuged briefly to remove precipitate. Supernatant was transferred to wells of a black 96-well plate (Corning, Corning NY) and read on a FlexStation 3 (Molecular Devices, Sunnyvale CA) with Ex/Em = 532/553 nm. Final results were calculated according to manufacturer instructions and final concentrations were reported as pmol MDA/μg total protein.

3.5.3. GSH/GSSG- Sample Preparation and Analysis

Approximately 20 mg of each tissue homogenate was resuspended in 400 μl of ice-cold PBS/0.5% NP-40. The tissue was homogenized with 10-15 passes in a Dounce homogenizer. Samples were centrifuged for 15 minutes at 4ºC at top speed in order to remove insoluble material. Deproteinization was carried out using trichloroacetic acid and sodium bicarbonate: one volume of ice-cold trichloroacetic acid was added into five volumes of sample, then vortexed briefly to mix well. After incubation on ice for 5-10 minutes, samples were centrifuged at 12,000 x g for 5 minutes at 4ºC. The supernatant was transferred to a fresh tube, recording the volume of each sample. On the day of assay, samples were neutralized by adding $NaHCO_3$ drop-by-drop to the supernatant until the pH reached 4-6 (measured using pH indicator paper). Samples were centrifuged at 13,000 x g for 15 minutes at 4ºC and supernatant collected. Once the samples have been deproteinized, neutralized, and free of trichloroacetic acid, supernatant was transferred to wells of a black 384-well plate (Corning, Corning NY). After 60-minute incubation at room temperature and protected from light, fluorescence was read on a FlexStation 3 (Molecular Devices, Sunnyvale CA) with Ex/Em = 490/520 nm. Final results were calculated according to the manufacturer instructions.

3.5.4. Histopathology- Sample Preparation and Analysis

Whole brains were collected at the time of euthanasia, and immediately immersed in 10% neutral buffered formalin. This allows for routine processing of neural tissues and other non-neural tissues. The fixed brain weight is then recorded. Relatively homologous levels defined by external landmarks were used for trimming while internal landmarks were used to select regions for analysis (Fig. 2; Table 1). Sections were cut at a thickness of 4-8um and paraffin embedded. The sections were stained with hematoxylin and eosin (H&E) and luxol fast blue (LFB) to identify affected neural structures.

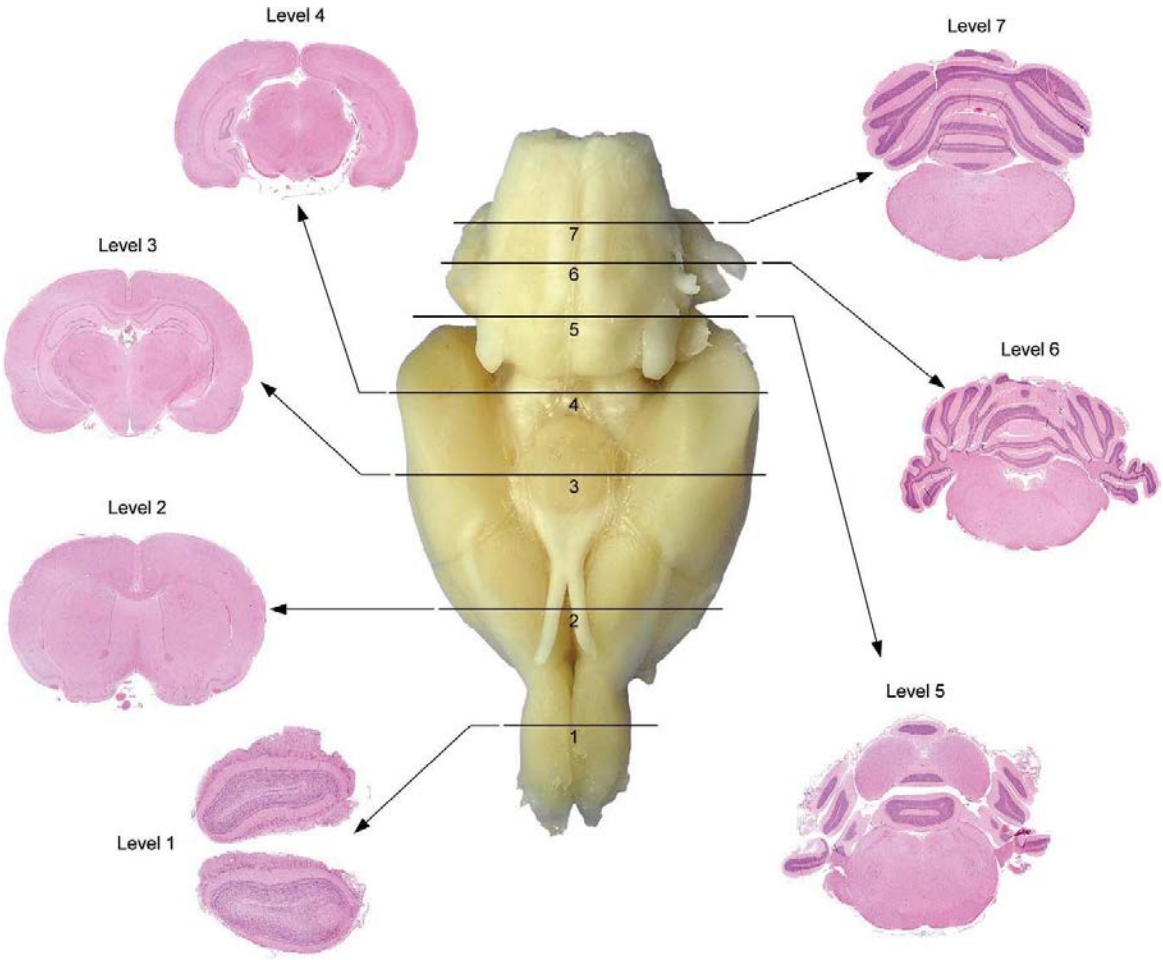

Figure 2. Trimming the adult rodent brain.

Representation of external landmarks on the ventral surface of the adult rat brain (central whole- organ image) used to consistently attain coronal sections with generally similar internal structures (peripheral H&E-stained sections) for neuro- pathology assessment during general toxicity studies. The solid black lines show where to place transverse cuts, and the black arrows point to the sections produced by trimming the brain in this manner. (Note: These trimming planes are used as an example. They are comparable to but not exactly identical to those demonstrated for the 7-level brain sampling scheme adopted recently by the U.S. National Toxicology Program [Rao et al. 2011]. Such differences are indicative of the modest variations in orientation and positioning of the brain sampling levels that should be expected among animals within a single study, across multiple studies, and among institutions.)

Table 1. Major landmarks for level orientation during brain sampling in adult rodents

Levels (from Figure 1)							
1	2	3	4	5	6	7	Brain structures (listed from rostral to caudal)
X							Olfactory bulb
	X						Anterior commissure
	X						Septal nuclei
	X						Caudate/putamen
	X	X	X				Cerebral cortex (frontal, parietal, temporal, occipital)
	X	X					Corpus callosum
	X	X					Internal capsule
	X	X					External capsule
		X					Optic tract
		X					Amygdala
		X	X				Hippocampus
		X					Thalamus
		X					Hypothalamus
		X	X				Cerebral peduncles
			X				Midbrain, rostral
				X			Midbrain, caudal
				X			Pons
				X	X	X	Pyramids
				X	X	X	Cerebellum
					X		Deep cerebellar nuclei
			X	X	X	X	Reticular formation
					X	X	Trigeminal nuclei and tracts
						X	Medulla oblongata
		X				X	Choroid plexus

Note: The table shows brain structures visible at given levels (using features visible when the organ is trimmed near the planes in Figure 2).

Six brain specimens from each treatment group (CTL, HYP, ALT) were analyzed for pathological changes. Levels 2, 3, 4, and 6 were examined for pathological change and assigned a score 0-5 using the severity grade scale shown in Table 2.

Table 2. Severity grade of pathologic change present in examined tissue

Grade	Term	Definitions	% Tissue Affected
0	Within Normal Limits (WNL)	Any histologic changes present are within normal limits	0
1	Minimal	Rare or inconspicuous lesions. Barely Exceeds WNL	< 5
2	Mild	Lesion is easily identified but of limited severity	6-25
3	Moderate	Lesion is prominent. Focal or multifocal lesion	26-40
4	Marked	Larger multifocal to coalescing lesion with potential for some loss of tissue structure	41-60
5	Severe	Extensive to diffuse lesion with potential for effacement of tissue structure	> 61

3.5.5. Electrophysiology- Sample Preparation and Analysis

Brain slice preparation

Rats were euthanized using rapid decapitation. Brain and brain slices were kept viable by maintaining them in ice-cold artificial cerebrospinal fluid (ACSF) that was kept continuously oxygenated (95/5 O_2/CO_2). ACSF consisted of (in mM): 124 NaCl, 3 KCl, 1.25 KH_2PO_4, 10 D-Glucose, 1 $MgSO_4$, 36 $NaHCO_3$, and 2 $CaCl_2$ (pH ~7.4). For hippocampal slices, cerebellum and approximately 1 cm of frontal cortex were removed and the remaining brain was sectioned at 350 µm thick using a vibratome (VT1000S Leica Microsystems) in the transverse plane, at approximately 30° laterally off the horizontal axis. Brain slices were maintained in warmed (37°C) oxygenated ACSF and allowed to recover for at least 60 min prior to recording. A new batch of ACSF was prepared each morning of experimentation and continuously oxygenated with 95% O_2 and 5% CO_2.

One hippocampal slice was placed onto the pre-coated microelectrode array probe, using a small weight to anchor the slice down. The probe containing the brain slice was then appropriately assembled with the QUAD II system, as specified in the instruction manual. A perfusion cap was used to circulate fresh oxygenated warmed ACSF into the probe and prevent the slices from drying. The flask containing the ACSF solution was continuously kept in a 37°C water bath. Flow rates of ACSF were adjusted such that the brain slice was constantly maintained in a liquid-air interphase. Typical flow rates range between 0.5 -1.0 ml/min. In order to deliver warmed, humidified oxygen to the brain slice, a line carrying 95% O_2 and 5% CO_2 was passed through a heated water-containing flask before entering the MED64 probe.

Electrophysiology recording

All electrophysiology data were obtained using AlphaMed's Quad II systems (Automate, Berkeley, CA). Probes were initially pretreated with 0.1% polyethylenimine (PEI) in 25-mM borate buffer for at least 24 hours prior to use. Data acquisition and stimulation protocols were performed using Mobius software (Automate, Berkeley, CA). A biphasic stimulating current of

10-100 µA was applied to the Schaffer collateral or the mossy fiber region of the hippocampus to obtain an input-output relationship curve. Evoked field potentials mainly consisting of inward deflections were recorded from neurons within the CA1 region of the hippocampus at a sampling frequency of 20 kHz using the Quad II multichannel amplifier, digitized and graphically displayed using Mobius software. Input-output data were obtained by delivering multiple biphasic stimuli at various intensities, ranging from 10 -100 µA. Paired pulse facilitation (PPF) were obtained by delivering sets of two consecutive stimuli of equal intensity that were 40 ms apart. Degrees of PPF were quantified by calculating the paired pulse (PP) ratio in which the response amplitude from the second stimulating pulse was divided by the response amplitude from the first pulse. Thus, a PP ratio of >1 indicates PPF whereas a PP ratio of <1 indicates paired pulse depression (PPD). Spontaneous spiking activity of neurons within the CA1 and CA3 region were recorded for 10 minutes and frequency of firing was calculated using the Mobius software. A threshold value of 5 times the standard deviation was used to calculate spike frequency.

For long term potentiation (LTP) experiments we use the input-output function to determine the size of the stimulating current that resulted in half of the maximal output response. Typically, a stimulating current size of 30-50 µA induced a half-maximal response and thus was used for our LTP experiments. Baseline recording was obtained for each slice for at least 20 min prior to LTP measurements. LTP was induced by delivering 3 trains of theta burst stimulation (TBS), consisting of 10 repeats of 4 high frequency stimulations (100Hz) every 200 ms to the Schaffer collateral regions. Evoked responses or field potentials (fEPSPs and population spikes) were monitored at 12-second intervals for at least 30 minutes following LTP induction. Percent potentiation was calculated by computing the percent difference in population spike amplitude or fEPSP slope at either 30 min following LTP induction by TBS from baseline. Averages of 10 data points were calculated to obtain baseline and LTP values.

Data analysis

Analyses of all data were performed using Mobius software. Microsoft Excel and Sigmaplot v.12.5 and v.13 were used to plot analyzed data and for statistical assessments. The downward (negative, inward) field potentials (fEPSP) were used to calculate degree of evoked response. In the input-output, paired pulse and LTP analyses, amplitudes and initial slopes of population spikes and field potentials were calculated to quantitate the size of evoked response. Amplitude and slope calculations were performed using Mobius software and Igor. Neuronal activity was recorded from typically 14 microelectrodes within the MED64 probe chamber. For any given slice, data obtained from multiple microelectrodes covering one defined brain region (eg. CA1) were averaged together to yield the response value for that particular slice. Statistical analyses were then performed on the data obtained from the different brain slices. Data are represented as means with the standard error of the mean (SEM) and were statistically compared using either a one-way or two-way analysis of variance (ANOVA). A calculated P of less than 0.05 is considered significantly different. All quantitation and statistical analysis as well as graphs were generated using Microsoft Excel and Sigmaplot v.12.5.

4.0 RESULTS

4.1 Proteomic Results

A shotgun proteomics approach was applied to quantitatively analyze global protein changes in four brain regions after the exposures. Protein abundances of six biological replicates for the exposure groups were compared using quantitative mass spectrometry. Table 3 summarizes total protein number detected in four brain regions at a false discovery rate of 5%. Results indicate that all brain regions showed similar amounts of identified protein groups as well as a similar number of significantly regulated proteins in all for exposure groups compared with control exposures. Between 0.09-2.3% of the total identified proteins were regulated (Table 3).

Table 3. Summary of identified and regulated proteins in brain

	Total	**HYP**	**ALT**
CX	2026	15	9
HC	1777	42	13
CB	2080	7	2
BS	2042	3	2

Hierarchical clustering analysis was performed on all identified proteins. Significantly regulated proteins were distinct between exposures groups and across brain regions with very little overlap (Figure 3).

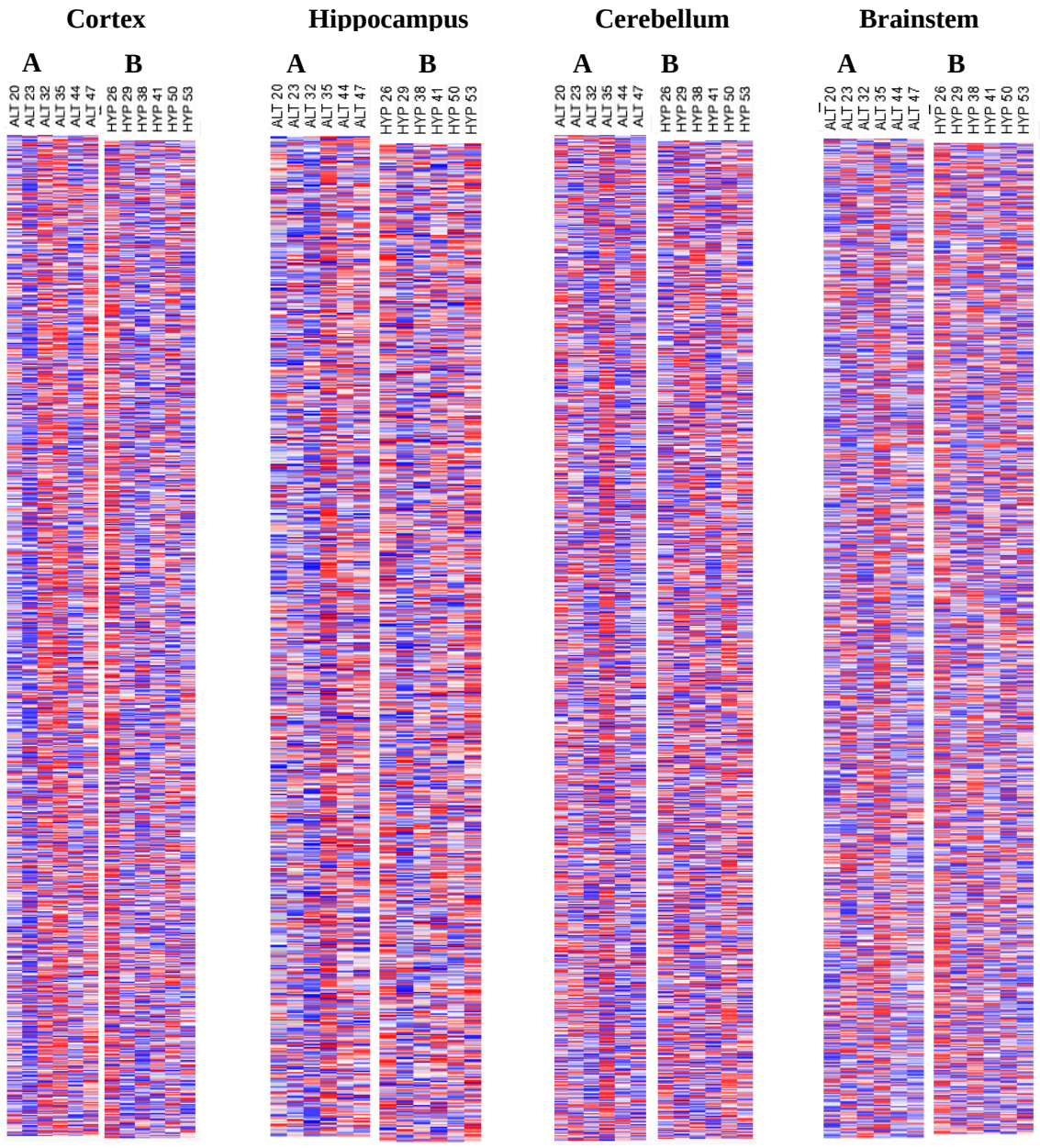

Figure 3. Hierarchical clustering of identified proteins

The heatmaps represent log_2 fold changes of all exposures vs CTL; blue - lower abundance; red - higher abundance. A) Animals underwent 8 hypobaric flights or B) 8 hyperoxic flights.

Exposure to HYP or ALT for different durations resulted in distinct protein profiles for significantly regulated proteins (Figure 4). The greatest number of significant changes in protein abundance was detected in HC, while CB and BS showed the lowest number of significant changes (absolute log_2 fold change $\geq|0.58|$, $p\leq0.05$).

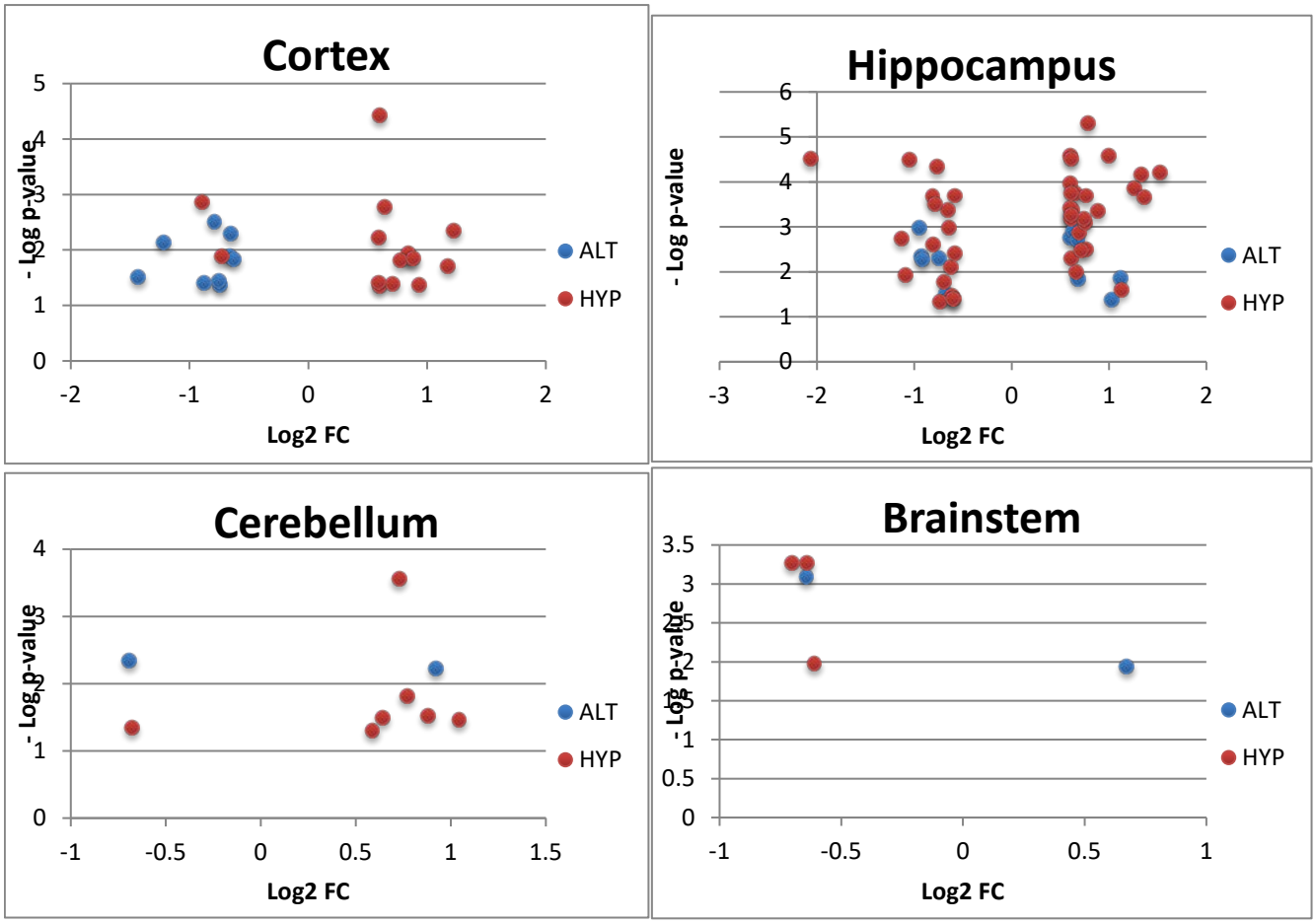

Figure 4. Distinct protein profiles in brain

Significant proteins were determined as having a $\log_2$ (fold change) greater than |0.585| as well as a p-value of 0.05 (-log (p-value) of 1.3). Only significant proteins are shown.

A list of all significantly regulated proteins per region and exposure is shown in Table 4. There was no overlap between regions.

Table 4. Proteins changes in all four brain regions after HYP or ALT exposures

Shown are protein name, gene name, and log_2 fold change of significantly regulated proteins with absolute log_2 fold change ≥0.58 and p≤0.05.

Protein name	Gene name	Log_2 FC
CX – ALT		
Sodium channel protein type 2 subunit alpha	Scn2a	-0.652
Inositol 1,4,5-trisphosphate receptor type 1	Itpr1	-1.221
Protein S100-A1	S100a1	-1.434
ADP-ribosylation factor 4	Arf4	-0.794
40S ribosomal protein S7	Rps7	-0.666
Phospholysine phosphohistidine inorganic pyrophosphate phosphatase	Lhpp	-0.745
Ras-related protein Rab-3B	Rab3b	-0.629
PRA1 family protein 3	Arl6ip5	-0.759
SH3 and multiple ankyrin repeat domains protein 2	Shank2	-0.881
CX – HYP		
Phosphatidylinositol 5-phosphate 4-kinase type-2 gamma	Pip4k2c	0.592
Tyrosine 3-monooxygenase	Th	0.865
Alpha-1-antiproteinase	Serpina1	0.600
GTPase HRas;GTPase HRas, N-terminally processed	Hras	0.598
Serine/threonine-protein kinase mTOR	Mtor	0.842
Maleylacetoacetate isomerase	Gstz1	0.931
Fibroblast growth factor 12	Fgf12	0.709
Neuron-specific calcium-binding protein hippocalcin	Hpca	-0.734
EF-hand domain-containing protein D2	Efhd2	-0.897
Eukaryotic translation initiation factor 3 subunit B	Eif3b	0.774
Ras-related protein Rap-1b	Rap1b	0.639
Isochorismatase domain-containing protein 1	Isoc1	1.223
Histone H3.1		1.173
Acid ceramidase	Asah1	0.881
Isoamyl acetate-hydrolyzing esterase 1 homolog	Iah1	0.589
HC – ALT		
Fumarylacetoacetate hydrolase domain-containing protein 2	Fahd2	-0.684
ELAV-like protein	Elavl1	-0.754
Inosine triphosphate pyrophosphatase	Itpa	0.601
Glutamate receptor 2	Gria2	0.660
Calcineurin subunit B type 1	Ppp3r1	1.109
High mobility group protein B1	Hmgb1	-0.952
Protein kinase C gamma type	Prkcg	0.623
cAMP-dependent protein kinase catalytic subunit beta	Prkacb	-0.928
Neuron-specific calcium-binding protein hippocalcin	Hpca	1.021
Limbic system-associated membrane protein	Lsamp	0.604
EH domain-containing protein 1	Ehd1	0.670
Inactive dipeptidyl peptidase 10	Dpp10	-0.920
Proteasome subunit beta type-7	Psmb7	0.681
HC – HYP		
ELAV-like protein	Elavl1	-0.815
Inosine triphosphate pyrophosphatase	Itpa	0.602
Protein S100-B	S100b	-0.632
60S ribosomal protein L7	Rpl7	-0.656
Cytochrome c oxidase subunit 6A1, mitochondrial	Cox6a1	-0.591
Non-specific lipid-transfer protein	Scp2	-0.771
Neurofilament heavy polypeptide	Nefh	0.994
Glutamate receptor 2	Gria2	0.781

Neurofilament light polypeptide	Nefl	0.606
Alpha-internexin	Ina	0.594
Metabotropic glutamate receptor 3	Grm3	-1.133
Syntaxin-1A	Stx1a	0.656
Matrin-3	Matr3	-0.590
Glial fibrillary acidic protein	Gfap	0.764
Gamma-aminobutyric acid receptor-associated protein-like 2	Gabarapl2	-0.697
Ras-related protein Rap-2b	Rap2b	0.608
Thymosin beta-4;Hematopoietic system regulatory peptide	Tmsb4x	1.256
Calcineurin subunit B type 1	Ppp3r1	1.352
High mobility group protein B1	Hmgb1	-0.793
Protein kinase C gamma type	Prkcg	0.684
Serine/threonine-protein phosphatase 2B catalytic subunit alpha isoform	Ppp3ca	0.646
cAMP-dependent protein kinase catalytic subunit beta	Prkacb	-1.057
Protein-tyrosine kinase 2-beta	Ptk2b	0.621
Neuron-specific calcium-binding protein hippocalcin	Hpca	1.522
Complexin-2	Cplx2	0.746
Core histone macro-H2A.1	H2afy	-0.614
Neurogranin;NEUG(55-78)	Nrgn	0.882
Brain acid soluble protein 1	Basp1	1.324
Ephexin-1	Ngef	-1.096
Cell cycle exit and neuronal differentiation protein 1	Cend1	0.761
Protein IMPACT	Impact	-0.652
Microtubule-associated protein 4	Map4	0.736
Astrocytic phosphoprotein PEA-15	Pea15	0.707
Limbic system-associated membrane protein	Lsamp	0.596
Tropomyosin alpha-3 chain	Tpm3	0.604
EH domain-containing protein 1	Ehd1	0.604
Plasma membrane calcium-transporting ATPase 4	Atp2b4	-0.737
Inactive dipeptidyl peptidase 10	Dpp10	-0.598
Cytochrome b-c1 complex subunit 8	Uqcrq	-2.067
Oxysterol-binding protein-related protein 1	Osbpl1a	-0.811
Glutaredoxin-1	Glrx	-0.608
Proteasome subunit beta type-7	Psmb7	1.119
CB -- ALT		
Glycolipid transfer protein	GLTP	-0.693
NEDD8	Nedd8	0.918
CB -- HYP		
Glutathione S-transferase alpha-3	Gsta3	0.726
Serine protease inhibitor A3K	Serpina3k	0.640
NADH-ubiquinone oxidoreductase chain 2	Mtnd2	-0.679
Enolase-phosphatase E1	Enoph1	0.585
NEDD8	Nedd8	1.041
Guanylate cyclase soluble subunit alpha-2	Gucy1a2	0.767
Latrophilin-3	Lphn3	0.877
BS -- ALT		
Opioid-binding protein/cell adhesion molecule	Opcml	-0.645
Protein kinase C gamma type	Prkcg	0.671
BS -- HYP		
Phosphatidylinositol 4-kinase alpha	Pi4ka	-0.613
Carboxypeptidase E	Cpe	-0.644
Opioid-binding protein/cell adhesion molecule	Opcml	-0.704

Biological processes after the HYP and ALT exposures in CX, HX, CB, and BS were investigated using Quiagen's Ingenuity Pathway Analysis. Gene ontology analysis was performed by combining all significantly regulated proteins for each exposure using the entire

human genome. Significantly regulated proteins are colored green for down-regulation, and red for up-regulation (Figure 5). Although the cortex and hippocampus show some trends for pathway regulation, the lack of clear, inclusive pathways indicate that the significantly regulated proteins in the brain stem and cerebellum are probably artifacts and not indicative of exposure effects.

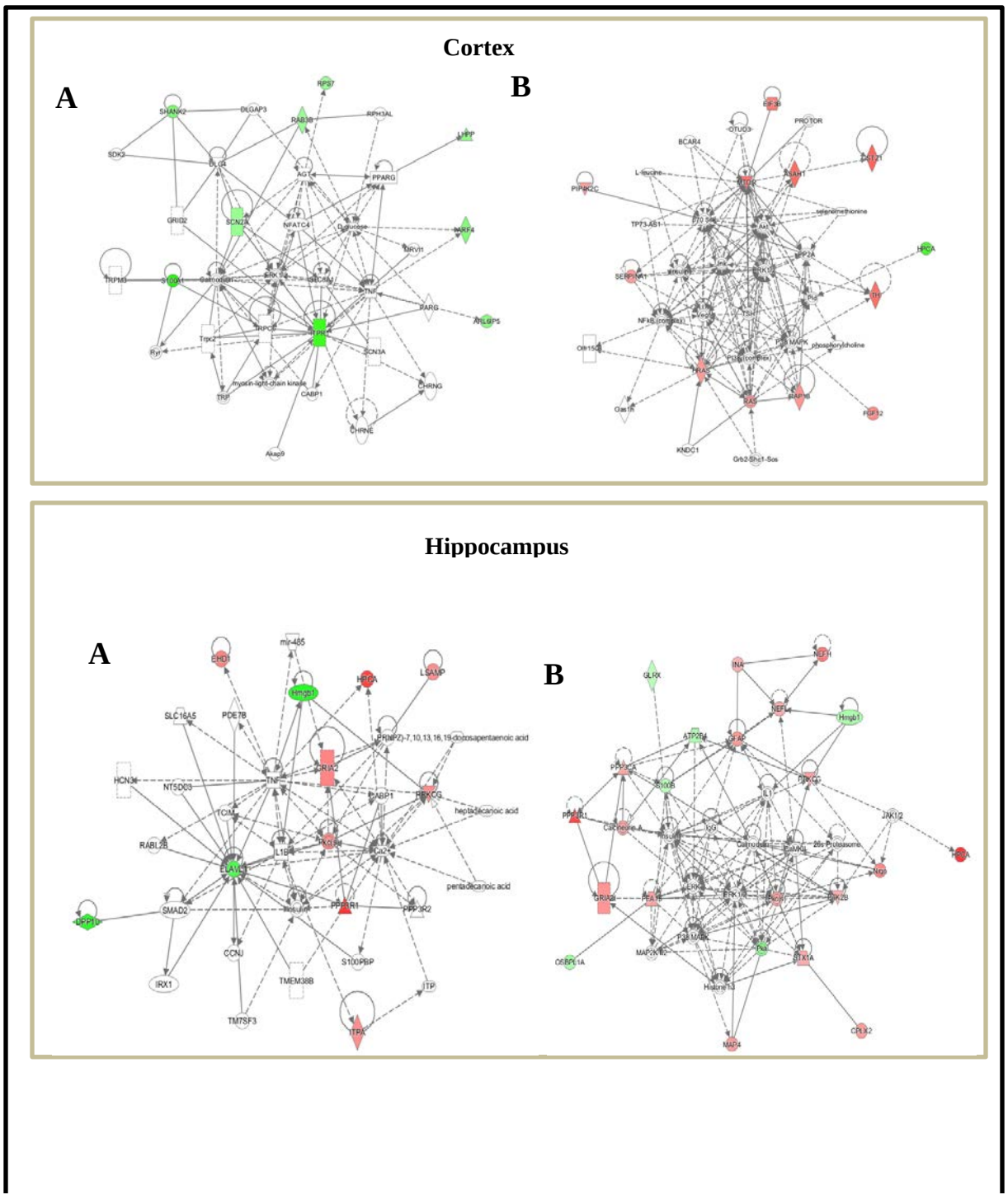

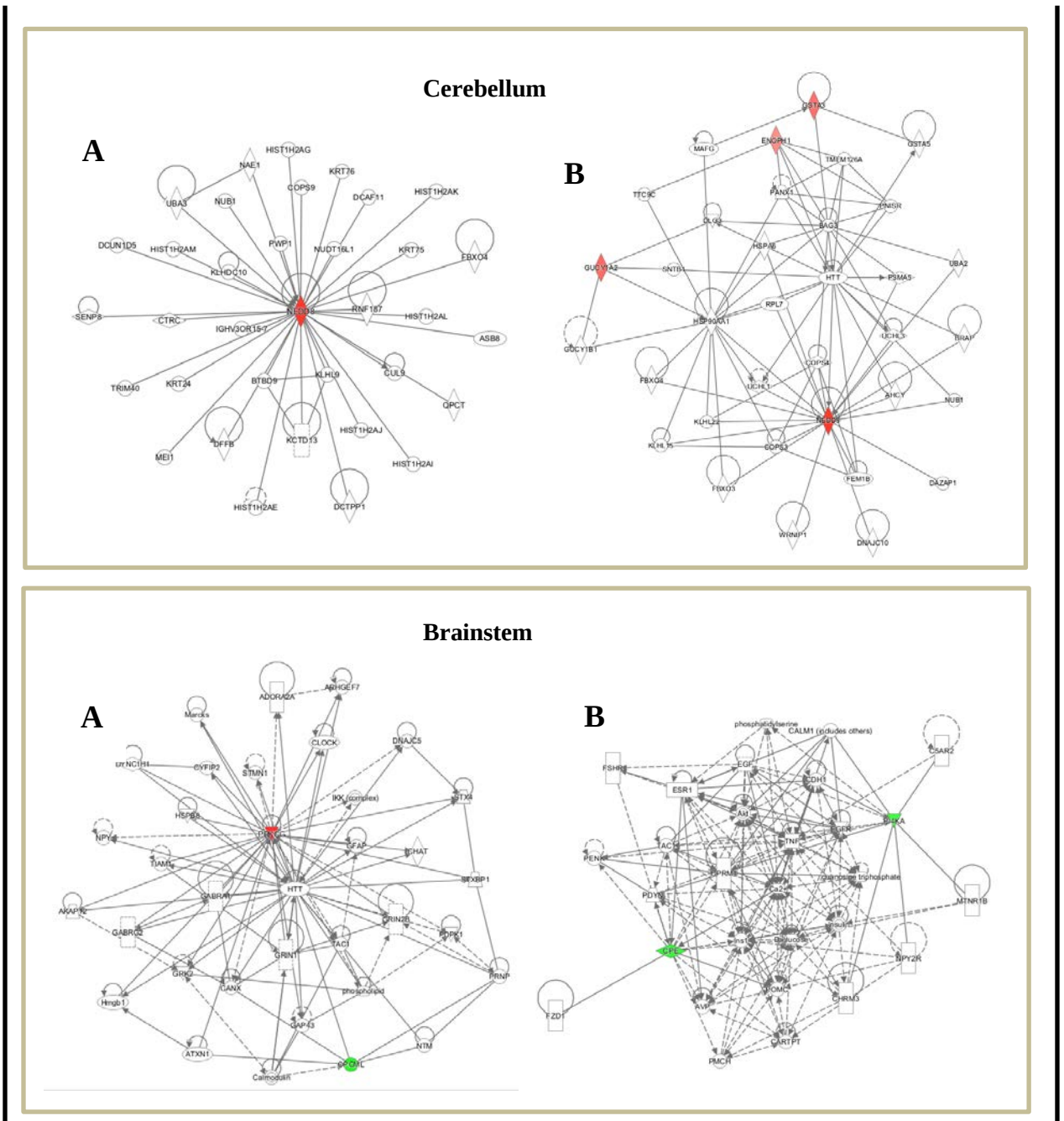

Figure 5. Biological pathways

Biological pathways after ALT or HYP exposures using gene ontology analysis through Ingenuity Pathway Analysis. A) Animals underwent 8 hypobaric flights, and B) 8 hyperoxic flights.

4.2 Metabolomic Results

Dual phase extracts were prepared from cerebellum (CB) and cortex (CX) brain samples from rats subjected to repeated conditions of hyperoxia ± hypobaria to stimulate high altitude flight experienced by U-2 pilots. The aqueous phase from the extract was lyophilized to dryness and is stored in a -80 °C freezer for future analysis if warranted. The lipid phase was analyzed using ^{13}C and ^{31}P NMR. The experimental groups and number of samples in each group are shown below.

(1) Control (CTL): ambient pressure + normoxic condition; n=6 rats, CX + CB; total # samples = 12
(2) Hyperoxia (HYP): ambient pressure + 100% O2; n=6 rats, CX + CB; total # samples = 12
(3) Altitude (ALT): pressure @ 30,000 ft altitude + 100% O2; n=6 rats, CX + CB; total # samples = 11 (sample 32CX was lost during preparation).

The ^{13}C and ^{31}P NMR spectra were acquired from all 35 samples. The cerebellum tissue weights were generally smaller than the cortex samples. Some cerebellum samples were <100 mg, and the ^{13}C NMR spectrum yielded very poor signal-to-noise (S/N) ratio. Thus, five cerebellum samples (Nos. 2, 26, 32, 35, 50) did not provide usable ^{13}C NMR data and were discarded from the analyses.

The baseline of each ^{13}C spectrum was corrected (flattened) using a 'rolling ball' algorithm, and the spectral regions containing solvent peaks (CDCl3 and MeOH) were zeroed. The data were then normalized using two methods. First, a 'sum normalization' was done such that the total intensity of all peaks in each spectrum sums to a constant value (1,000). Second, normalization of the spectral intensities to the tissue weight for each sample were calculated. These methods will help account for differences in signal amplitudes due to variations in sample size. The normalized spectra were then binned (186 bins) as a means of data reduction for multivariate data analyses. The binned data were then used as input to Principle Components Analysis (PCA) to visualize the data and determine whether there are distinct metabolite profiles or patterns within tissues and experimental groups.

Figure 6 shows PCA scores plot (PCA vs. PC2) for all samples, which are labeled by tissue type (cerebellum, CB; cortex, CX). The data were autoscaled using all samples as reference. This plot clearly shows unique patterns for each tissue representing differences in the lipid profiles for cerebellum and cortex. There is a clear separation in data along PC1, which accounts for 95% of the total variance. Indeed, the Davies-Bouldin (DB) index for this analysis is 0.03. The DB index is a metric used to evaluate clustering algorithms and is calculated as the ratio of 'within cluster scatter' to 'between cluster separation', and its value is similar to a p-value statistic. It is not surprising that these two brain regions display different lipid profiles.

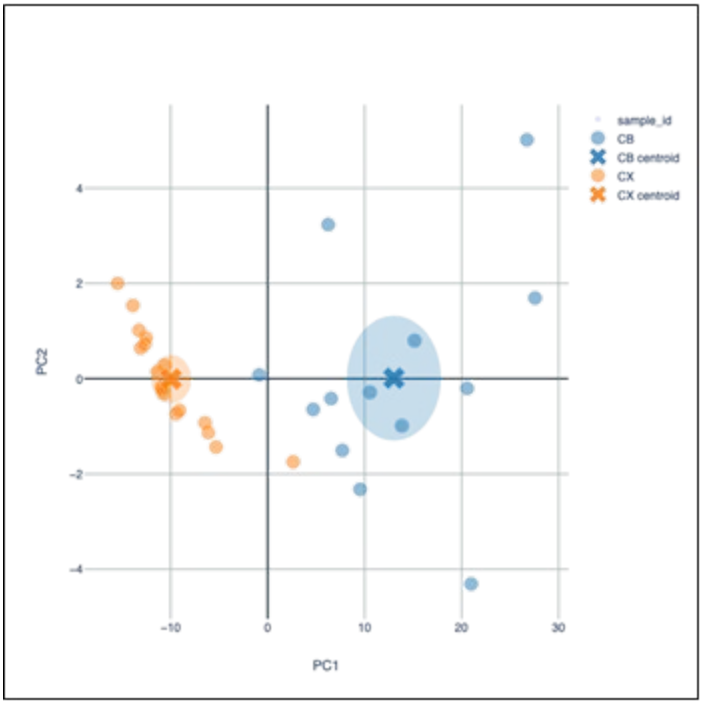

Figure 6. PCA scores plot (PC1 vs. PC2) for ^{13}C spectra of lipid extract modeling all groups and atuoscaled using all samples as reference

Samples separate by tissue type, CB and CX, shown in blue and orange, respectively. The centroid mean ± 2 SEM is marked by an "X" and shaded cloud for CB and CX samples. Data were autoscaled relative to all samples as reference. CB and CX samples show distinct lipid metabolite profiles (Davies-Bouldin index is 0.03).

This same analysis (PCA modeling all data) was also conducted after autoscaling the data using either CB samples or CX samples as reference. The scores plots are shown in Figure 7. Again the two tissue types separate in PCA space, indicating distinct metabolite profiles. In fact, the separation is much better when the data are scaled to each individual tissue type rather than all data, as indicated by the larger PC1 range (compare the PC ranges in Figs. 6 and 7). This is particularly true for the data scaled to CX. In Figure 8, we show this same PCA plot (modeling all data and autoscaling to the CX samples), but now the data points are color-coded to identify the specific experimental groups. The CX data are very tightly clustered but the CB data are more greatly dispersed over PC-space. Also, note that CB samples for two ALT animals (#20 and 23) are well separated from the CTL data points. These may represent rats that were more sensitive to the hyperoxia/hypobaria treatment.

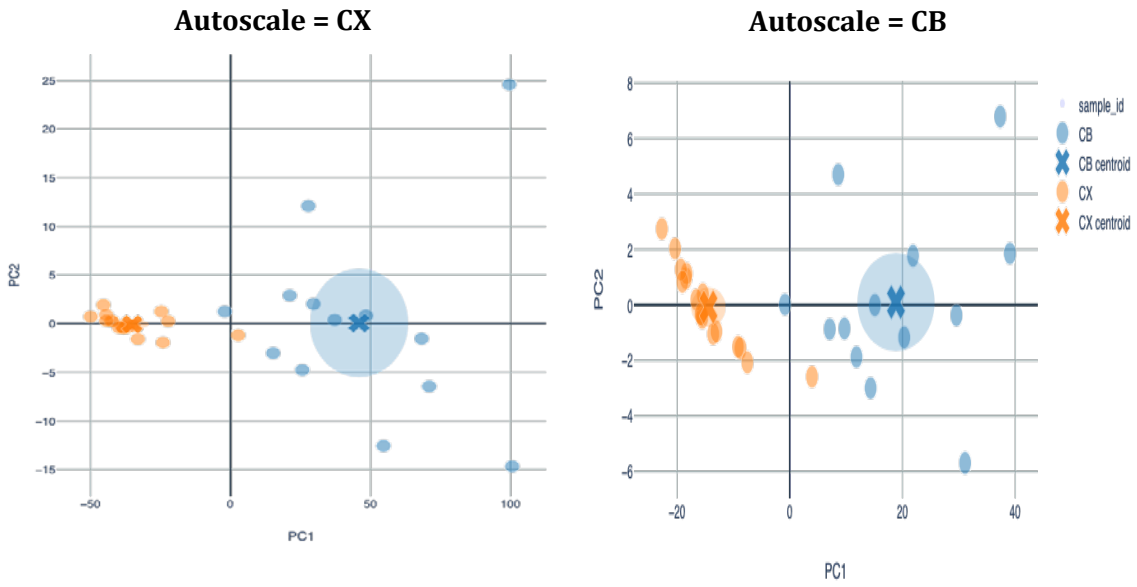

Figure 7. PCA scores plots (PC1 *vs.* PC2) modeling all groups for CB (blue) and CX (orange) with data atuoscaled using either CB data as reference (right panel) or CX data as reference (left panel)

The centroid mean ±2SEM is indicated by the "X" and shaded cloud for CB and CX data.

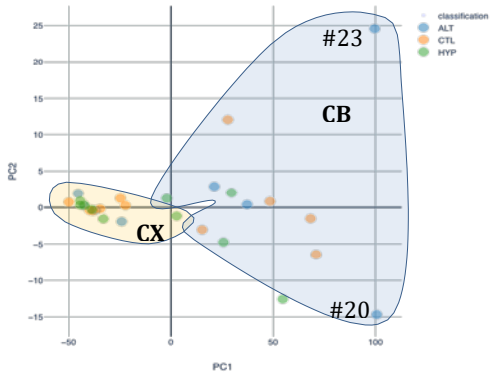

Figure 8. PCA scores plot (PC1 *vs.* PC2) modeling all groups in both CB and CX samples with data autoscaled to the CX data (identical to Fig. 7; left panel).

Samples within each tissue type are outlined within the shaded boundary and data points indicate rats belonging to the ALT (blue), HYP (green), and CTL (orange) groups. Two ALT animals (#20 and 23) from the CB samples are well separated from all other data and may represent sensitive responders to treatments.

Next, a PCA was conducted to determine whether there are any observed differences in metabolite patterns for the three experimental groups (CTL, HYP, ALT) by focusing the analysis within each tissue type. These PCA scores plots are shown in Figure 9 for cerebellum and cortex

samples. Each tissue type was autoscaled separately (i.e., CB samples were autoscaled using all CB groups as reference, while CX samples were autoscaled using all CX group as reference). There does not appear to be any distinct patterns among the experimental groups in either tissue type. The data points are randomly scattered among all experimental animals, and the error boundaries (±2 SEM) are overlapping for each group. It is interesting, however, that one HYP sample (#38) and one ALT sample (#20) plot well outside of the error boundaries in both CB and CX samples. These specific animals may have responded to the exposures differently than others in the group. In other words, it is likely that some animals may be more sensitive to the hypobaria/hyperoxia treatment and, therefore, we are observing differential responses to exposure. But we caution that this same finding is also true for the control animals (CTL), so the ALT and HYP samples do not appear to be greatly different from controls.

Any potential patterns in the data could be discerned by autoscaling using different groups as reference, and by modeling the PCA by group pairs (CTL vs. ALT and CTL vs. HYP), rather than including all three groups in the PCA model. For example, this could be done by autoscaling the CB data using only the CB-CTL group as reference. This was also done for the cortex samples. But the results did not change. For all analyses, the data show a large scatter with all group means overlapping, regardless of the autoscale referencing procedure or modeling parameters (data not shown). There are no distinct differences between any of these experimental groups. Since the PCA for the 13C lipid datasets do not show any specific patterns between experimental groups, a discriminate analysis (OPLS-DA) was not warranted. Also, an examination of the ^{13}C NMR spectra of lipid extracts visually in the region containing the C18-methyl carbon of cholesterol (at ~12 ppm) was made. In the previous 'U-2 study' (conducted in 2017), there were other peaks in this region in some animals that were tentatively attributed to oxidized products from cholesterol metabolism. Therefore, careful investigation ensued of this region of the ^{13}C spectrum in all samples from the present study, and no presence of additional 'unknown' peaks was found. The only peak observed was the C18 carbon of cholesterol at 12.4 ppm.

Taken together, the phospholipid analysis (*via* ^{31}P NMR) and the more general lipid analysis offered by ^{13}C NMR, indicate that exposing rats to hypobaria and/or hyperoxia appears to have no significant effects on brain lipid metabolite profiles measured in cerebellum or cortex. There is some weak evidence, however, that one animal in the ALT group (#20) and one animal in the HYP group (#38) may show some slight differences in the lipids present in CB and CX samples (Figure 9). But there are also at least two control samples that show this same displacement from the centroid group mean. Overall, there does not appear to be any real significant differences in the brain lipid metabolite profiles among the experimental groups.

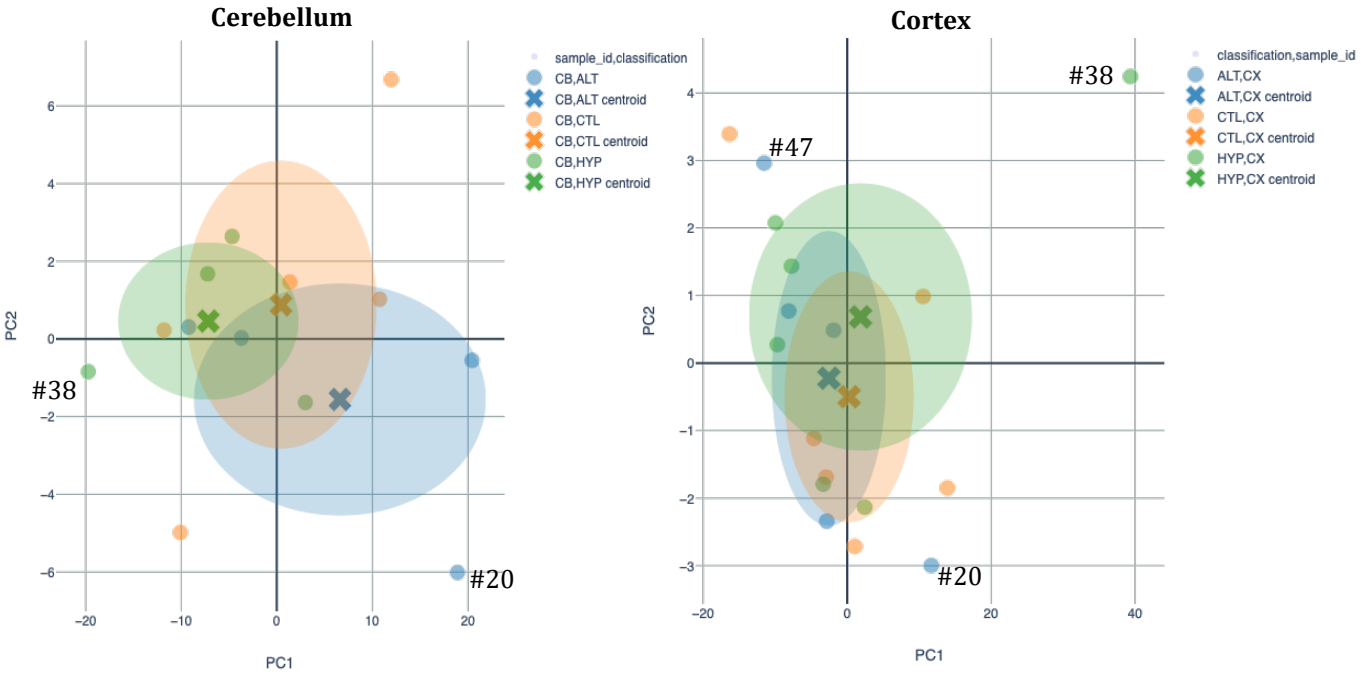

Figure 9. PCA scores plots for each tissue (CB and CX) identifying samples belonging to the CTL (orange), HYP (green), and ALT (blue) experimental groups

Cerebellum samples were autoscaled using all CB groups as reference, while cortex samples were autoscaled using all CX groups as reference. The centroid mean ±2SEM is marked by an "X" and associated color-cloud for each experimental group. Some subject IDs are identified in the plots for specific HYP and ALT samples that lie outside the error boundaries for the group.

4.2.1. Metabolomic Results: Phospholipids

All ^{31}P NMR spectra were processed as follows: Fourier transform, phase correction, baseline correction, and spectral peak-fitting. This final step fits the spectral peaks to a Lorentzian function and yields integrated intensities for all signals. Although all major phospholipid signals were assigned, some peaks in the spectra remained unassigned (generally weaker signals). There were some differences in the observable peaks for the cortex and cerebellum samples. For example, lyso-phosphatidylethanolamine was observable in four cerebellum samples, but only two cortex samples, while an unidentified peak at 0.834 ppm was observed in five cortex samples but none of the cerebellum samples. A representative spectrum of the cortex is shown in Figure 10.

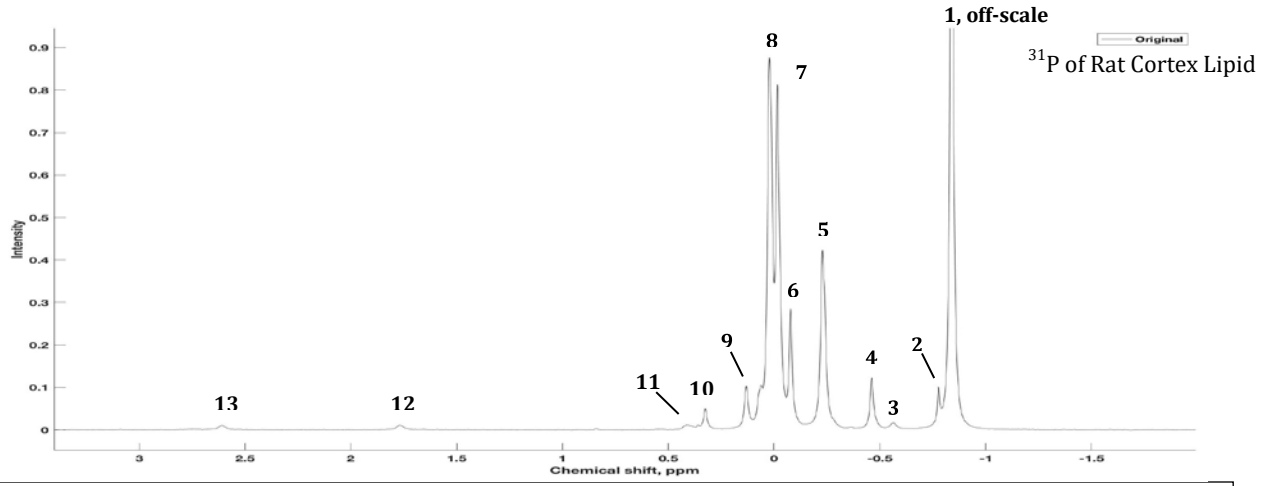

Figure 10. ^{31}P NMR spectrum of a rat cortex (sample #14) lipid extract at 14.2 T

The chemical shift reference was set on PC (#1 at -0.84 ppm). The vertical scale is expanded to show weaker signals, making PC plot off-scale. Peaks are identified by numbers as follows: 1, PC; 2, PC-Pls; 3, LPC; 4, PI; 5; 6, SM; 7, PE; 8, PE-Pls; 9, CL; 10, PA; 11, PG; 12 & 13, unknown. Abbreviation are given in Table 5.

The chemical shift for phospholipid resonances are a function of sample composition, therefore, peak positions can vary among samples making it difficult to unequivocally assign all resonances. Multiple experiments were conducted using phospholipid standards to help with peak assignments. Samples were prepared with individual phospholipids (PL) and mixtures of PL, and we "spiked" some of the tissue extracts with standards to confirm peak assignments in real tissue samples. Spectra were 'aligned' from these 35 rat brain tissue samples in an attempt to match the phospholipid peaks between samples. This has resulted in definitive assignments for 12 metabolites. In addition, there were 4 - 5 unidentified peaks in some of these spectra. Two of these peaks at 1.69 and 2.52 ppm were always observed and were quantified in all samples, but the origins of these signals is unkown. Other unidentified peaks at 0.334, 0.371, and 0.834 ppm were observed in some samples and were also quantified.

Absolute quantitation of metabolites was accomplished by addition of triphenylphosphate (TPP) as an internal reference standard at a known concentration. Intensities for all NMR resonances had to be corrected for T1 saturation and NOE spectral effects (since spectra were acquired under saturating conditions with proton decoupling). This was accomplished by acquiring two spectra for a representative sample: (1) using our normal acquisition parameters, and (2) using acquisition parameters that allow for full T1 relaxation without NOE. The relative change in signal intensities is measured for each peak of interest, which is expressed as a ratio (a saturation factor). This experiment was repeated for several samples, including both cerebellum and cortex samples, and averaged the results for the measured saturation factor (SF). The SF for each metabolite resonance was used to correct spectral intensities for T1 saturation and NOE effects. The number of equivalent phosphorus atoms in each metabolite was also accounted for (i.e., phosphatidylcholine has one P, but cardiolipin has two P). NOTE: a saturation factor for three resonances were not able to be measured because these peaks were weak and not always observed in the spectra. Thus the quantities for lyso-phosphatidylcholine, lyso-phosphatidylethanolamine, and U- 834 (an unidentified peak at 0.834 ppm) represent relative

intensities and are not true umol/g tissue values (for these peaks, the SF was set to 1.00). But regardless of this detail, these metabolite signals should be comparable between samples. Also, the lyso-phosphatidylcholine (LPC) species were measured from the sum of three peaks (-0.567, -0.324, and -0.237 ppm) determined to be from sn-1 and sn-2 LPC species (based on our studies using PL standards).

The quantified metabolite concentrations for all three groups in both cerebellum and cortex are shown in Table 5. Also listed are the n-values for these measurements, to indicate which peaks were routinely observed versus those that were observed in only a few samples. Note that U-834 was not observed in any of the cerebellum samples, and was only observed in 5-out-of-17 cortex samples. So even though the value for this metabolite in the HYP group is 2-times the CTL value, the sample size is too small to be statistically significant.

Table 5. Concentrations of phospholipids measured by ^{31}P NMR in lipid extracts from rat cerebellum and cortex samples

*Values are expressed as μmol/g tissue (Mean ± SE) for all three experimental groups (CTL, HYP, ALT), with the exception of LPC, LPE, and U834 species. True concentration values for these metabolites (indicated by an asterisk, *) was not possible since saturation factors for the NMR signals could not be measured. Therefore, the values for LPC and LPE are relative intensities, which can be compared between samples, but are not absolute concentrations. Some peaks were not observed in all samples; n-values are given in (). Within each tissue type, there were no significant differences between groups for any of the phospholipids measured (ANOVA, p < 0.05). Abbreviations are given in the footnote.*

	Cerebellum: Mean ± SE (n-value)			Cortex: Mean ± SE (n-value)		
PL	**CTL**	**HYP**	**ALT**	**CTL**	**HYP**	**ALT**
PC	18.5 ± 1.8 (6)	15.7 ± 0.8 (6)	18.1 ± 0.7 (6)	15.2 ± 1.1 (6)	14.8 ± 0.93 (6)	14.0 ± 0.3 (5)
PC-Pls	0.7 ± 0.1 (6)	0.8 ± 0.1 (6)	0.9 ± 0.1 (6)	0.5 ± 0.04 (6)	0.4 ± 0.04 (6)	0.5 ± 0.05 (5)
PI	1.1 ± 0.1 (6)	1.0 ± 0.05 (6)	1.0 ± 0.1 (6)	0.9 ± 0.09 (6)	0.9 ± 0.07 (6)	0.8 ± 0.03 (5)
LPC species *	0.3 ± 0.04 (5)	0.3 ± 0.03 (3)	0.2 ± 0.02 (3)	3.3 ± 1.0 (6)	2.5 ± 1.1 (6)	3.9 ± 0.9 (5)
PS	5.6 ± 0.6 (6)	4.9 ± 0.2 (6)	5.6 ± 0.2 (6)	2.8 ± 0.9 (6)	3.2 ± 0.8 (6)	2.2 ± 0.7 (4)
SM	2.6 ± 0.3 (6)	2.2 ± 0.1 (6)	2.5 ± 0.1 (6)	1.8 ± 0.5 (2)	1.6 ± 0.1 (3)	1.3 ± 0.1 (2)
PE	7.2 ± 0.7 (6)	6.1 ± 0.4 (6)	6.9 ± 0.3 (6)	6.7 ± 0.5 (6)	6.7 ± 0.4 (6)	7.7 ± 1.4 (5)
PE-Pls	15.1 ± 1.4 (6)	13.2 ± 0.5 (6)	14.7 ± 0.7 (6)	9.6 ± 0.7 (6)	9.3 ± 0.6 (6)	11.0 ± 1.9 (5)
CL	0.3 ± 0.1 (5)	0.3 ± 0.1 (6)	0.4 ± 0.1 (6)	0.4 ± 0.04 (6)	0.4 ± 0.03 (6)	0.3 ± 0.07 (5)
PA	0.6 ± 0.1 (6)	0.5 ± 0.03 (6)	0.6 ± 0.04 (6)	0.4 ± 0.02 (6)	0.4 ± 0.05 (6)	0.4 ± 0.02 (5)
U-334	0.05 ± 0.02 (5)	0.05 ± 0.01 (4)	0.05 ± 0.01 (3)	0.09 ± 0.06 (6)	0.03 ± 0.01 (5)	0.04 ± 0.01 (3)
U-371	0.1 ± 0.02 (5)	0.06 ± 0.02 (4)	0.06 ± 0.01 (3)	0.04 ± 0.01 (6)	0.05 ± 0.01 (5)	0.05 ± 0.01 (3)
PG	0.1 ± 0.02 (5)	0.1 ± 0.02 (4)	0.2 ± 0.1 (4)	0.1 ± 0.04 (6)	0.1 ± 0.03 (5)	0.1 ± 0.02 (3)
LPE species *	0.2 (1)	0.03 (1)	0.2 ± 0.2 (2)	0.03 ± 0.02 (2)	(0)	(0)
U-169	0.3 ± 0.1 (5)	0.2 ± 0.02 (5)	0.2 ± 0.04 (3)	0.2 ± 0.03 (6)	0.2 ± 0.02 (5)	0.2 ± 0.02 (4)
U-253	0.4 ± 0.05 (5)	0.3 ± 0.03 (5)	0.3 ± 0.02 (3)	0.2 ± 0.02 (6)	0.2 ± 0.03 (5)	0.2 ± 0.04 (4)
U-834 *	—	—	—	0.02 ± 0.01 (2)	0.04 ± 0.02 (3)	(0)

Abbreviations: PC, phosphatidylcholine; PC-Pls, phosphatidylcholine plasmalogen; PI, phosphatidylinositol; LPC, lyso-phosphatidylcholine; PS, phosphatidylserine; SM, sphingomyelin; PE, phosphatidylethanolamine; PE-=Pls, phosphatidylethanolamine plasmalogen; CL, cardiolipin; PA, phosphatidic acid; PG, phosphatidylglycerol; LPE, lyso-phosphatidylethanolamine; U, unidentified with peaks at: 0.334, 0.371, 0.834, 1.69, and 2.53 ppm.

An ANOVA was conducted for each phospholipid metabolite to assess differences between experimental groups. No statistical difference were observed ($p < 0.05$). The results are displayed graphically in Figures 11 and 12.

Figures 11 and 12 show bargraphs of the metabolite concentrations listed in Table 5 for the cerebellum and cortex, respectively. As mentioned above, there are no statistical difference between groups in the cerebellum or cortex for any of these phospholipid metabolites (ANOVA; $p<0.05$). Statistical analyses could not be conducted for the LPE species due to low *n*-values

since these signals were not observable in all samples. The LPC species were more prevalent in the cortex samples where both 1-lyso-PC (at -0.57 ppm) and 2-lyso-PC signals (at -0.32 and -0.24 ppm) were observable. In order to obtain a composite value for LPC-species in cortex, these peak areas were summed. By contrast, only 1-lyso-PC was observed in the cerebellum from 11 of 18 samples. Therefore, these data were not reported in Fig. 2 because this signal was only observed in six of the treated rats (3 HYP and 3 ALT). An increase in lyso-phospholipid species might be indicative of oxidative damage to membranes, but these results appear to be very variable and the low sample size in this study prohibits any definitive assessment.

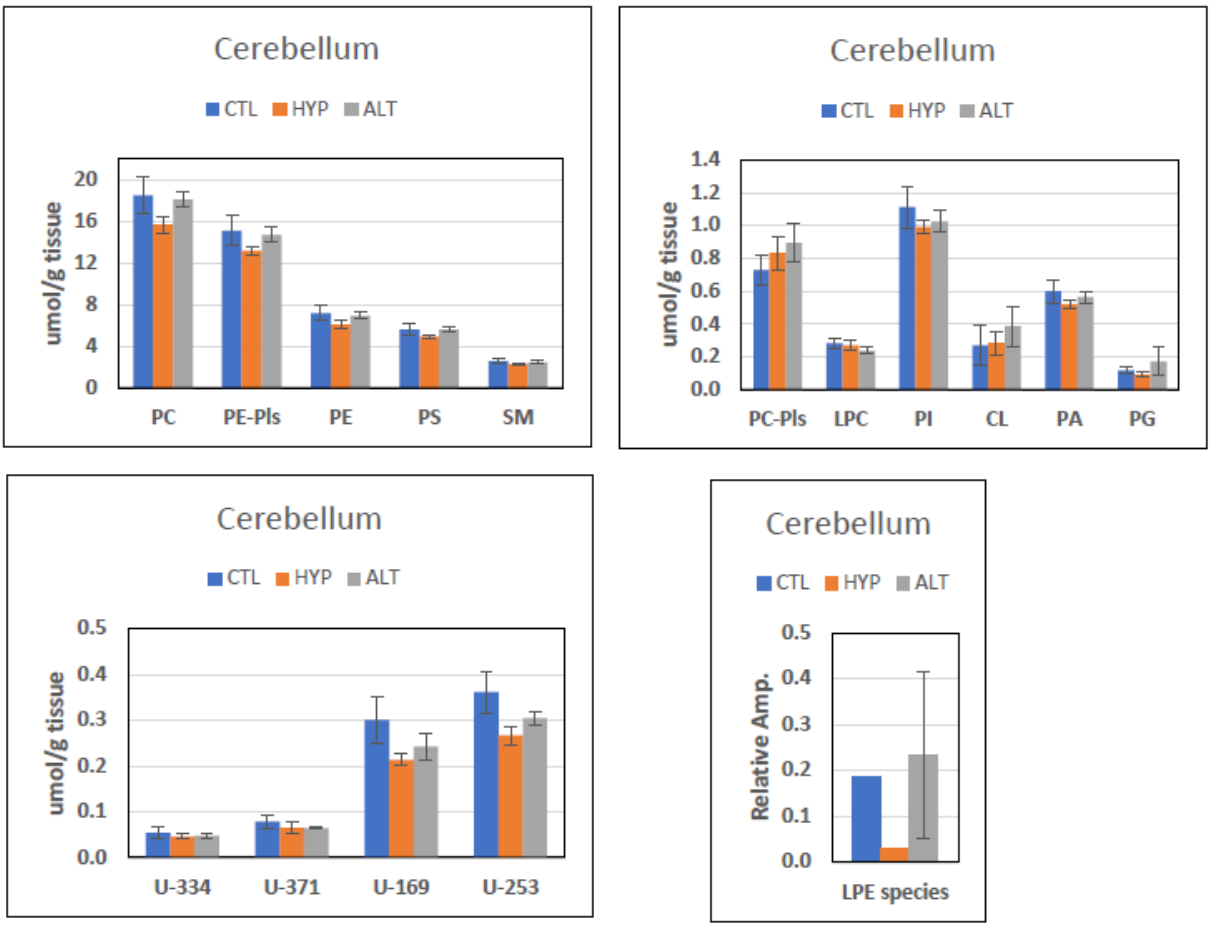

Figure 11. Comparison of phospholipid metabolites measured by ^{31}P NMR in cerebellum from rats for the CTL, HYP, and ALT groups

Phospholipids were quantified and are reported in □mol/g tissue (Mean ± SE), except for LPE species, for which we were unable to measure the saturation factor to correct NMR intensities for absolute quantification. Data are presented in four plots with appropriate scaling to help visualize high and low abundance metabolites. Abbreviations are listed in Table 1. There are no statistical differences between CTL, HYP, and ALT groups for any of these metabolites.

An analysis of these same data was conducted by calculating the amount of each phospholipid represented as a percentage of the total pool size. These results for cerebellum and cortex are shown graphically in Figure 13. Again there are no differences in the distribution of phospholipid metabolites between CTL, HYP, and ALT groups.

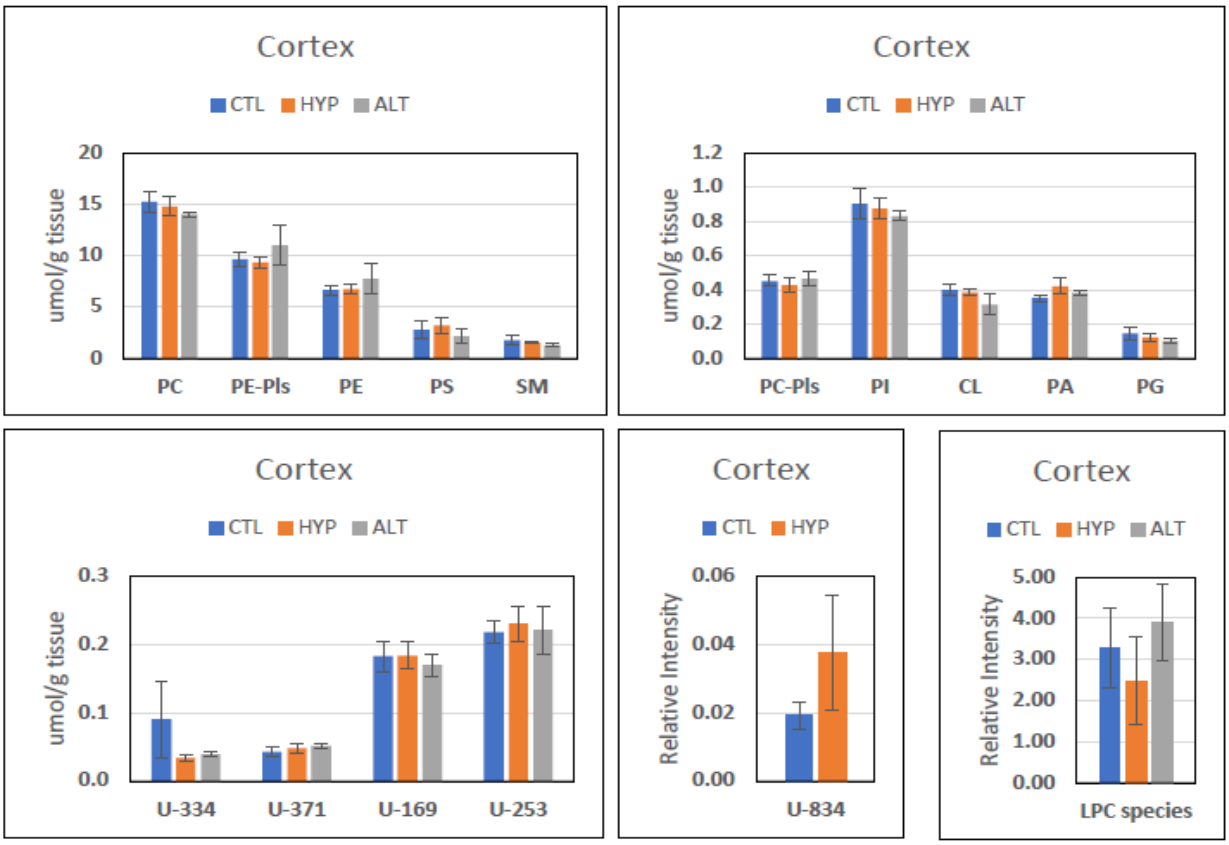

Figure 12. Comparison of phospholipid metabolites measured by ^{31}P NMR in cortex from rats for the CTL, HYP, and ALT groups

Phospholipids were quantified and are reported in μmol/g tissue (Mean ± SE), except for U-834 and LPC species, for which we were unable to measure the saturation factor to correct NMR intensities for absolute quantification. The U-834 metabolite was not observed in any of the ALT samples. Data are presented in multiple plots with appropriate scaling to help visualize high and low abundance metabolites. Abbreviations are listed in Table 1. There are no statistical differences between CTL, HYP, and ALT groups for any of these metabolites.

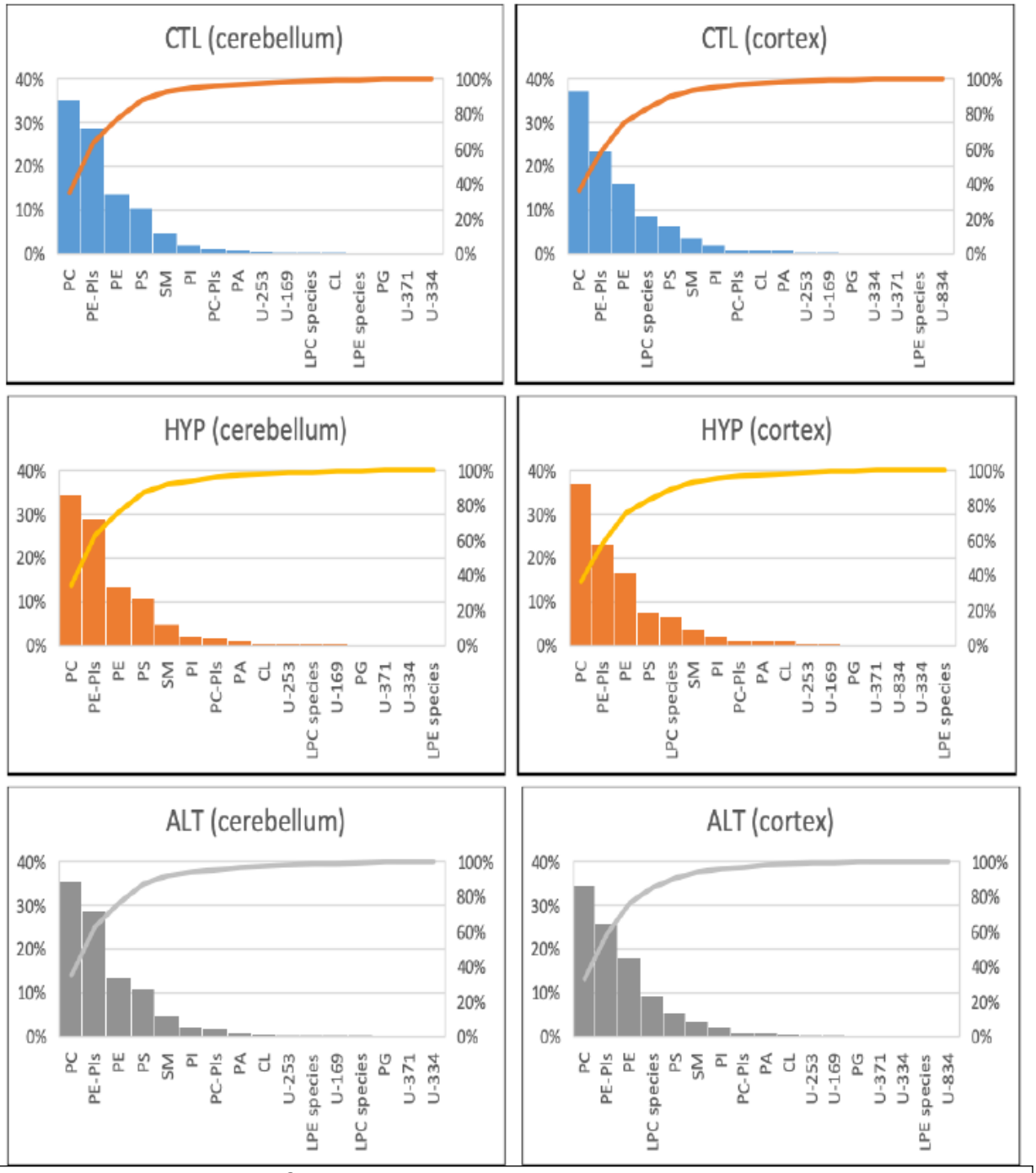

Figure 13. Contribution of each phospholipid species to the total phospholipid pool size measured by ^{31}P NMR in cerebellum and cortex samples from CTL, HYP, and ALT groups (Mean ± SE)

The percentage of each metabolite (left-hand axis) and the added contribution to the phospholipid pool (right-hand axis) is shown in the line graph. There are no apparent differences between groups within each brain region.

4.2.2. Metabolomic Results: Lipids via ^{13}C NMR

The lipid extracts samples were also analyzed by ^{13}C NMR, however, this nuclide has much lower sensitivity than ^{31}P, and some problems were encountered with the small tissue size for cerebellum samples. A representative spectrum for the cortex is shown in Figure 14. Five of the cerebellum samples (#2, 26, 32, 35 and 50) yielded very poor signal-to-noise ratio, where many resonances were notnobservable. Therefore, these samples were not included in our analyses.

The ^{13}C NMR spectra were analyzed using multivariant data analysis techniques. First, spectra were Fourier transformed, phased, and then upload to a server in the Bioinformatics Research Group (BiRG) at Wright State University. The BiRG is directed by Dr. Michael Raymer (Department of Computer Science) and contains various toolkits for NMR-based metabolomics analyses that our laboratories have developed in collaboration.

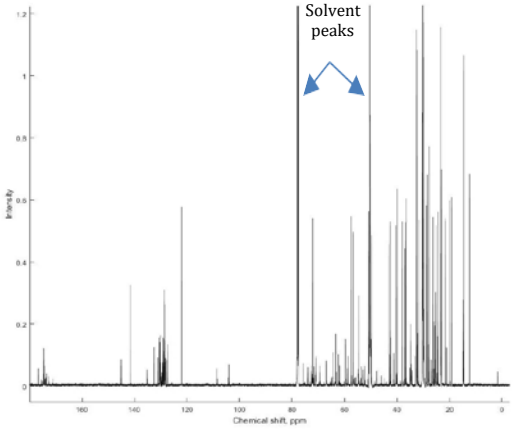

Figure 14. Representative ^{13}C NMR spectrum of a rat cortex lipid extract

The solvent peaks (arrows) are CDCl3 and MeOH.

4.3 General and Oxidative Stress Assay Results

A variety of biochemical assays were completed to characterize the levels of general or oxidative stress caused by exposure to hyperoxia or altitude relative to control. Corticosterone was measured in serum to quantify the level of generalized stress. MDA is a product of lipid peroxidation and is a marker of oxidative stress. Glutathione exists in its reduced (GSH) and oxidized (GSSG) forms, and an increased GSSG-to-GSH ratio is indicative of oxidative stress.

Corticosterone levels were surveyed in serum from control and exposed rats (Figure 15). The ALT group showed a statistically significant increase above control indicating increased stress in those animals. The HYP group did not show a statistically significant increase, however, a trend towards increased corticosterone levels was observed.

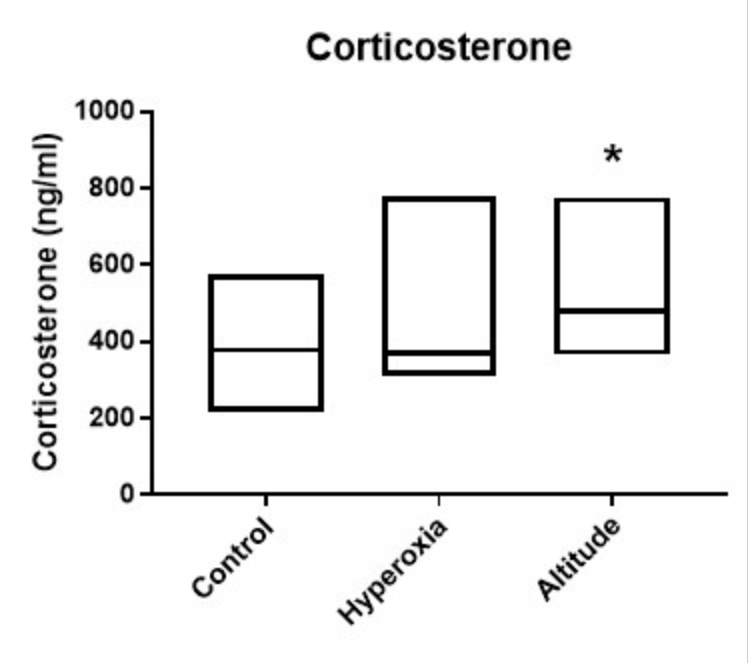

Figure 15. Serum levels of corticosterone. Levels of corticosterone as a marker of general stress in hyperoxic (HYP) and hypobaric (ALT) conditions relative to control

*Data are mean ± SD. (n=12 for all groups, * p≤0.05 relative to control)*

MDA was assayed in all brain regions except hippocampus. In cerebellum, levels of MDA were no different in either treatment group relative to control (Figure 16), yet variability was high. Levels of MDA were significantly higher ($p<0.05$) in cortex from the hyperoxia group as compared to control**.** In brainstem, when rats were exposed to hypobaria (ALT), levels of MDA decrease significantly relative to control ($p=0.0465$). In addition, MDA levels differed significantly between hypobaric (ALT) and hyperoxia (HYP) ($p=0.0334$). Levels of the reduced (GSH) and oxidized (GSSH) forms of glutathione were measured in brain cortex tissues and lung tissue (Figure 17). No differences were observed in brain tissue or lung tissue between the exposure groups as compared to the control.

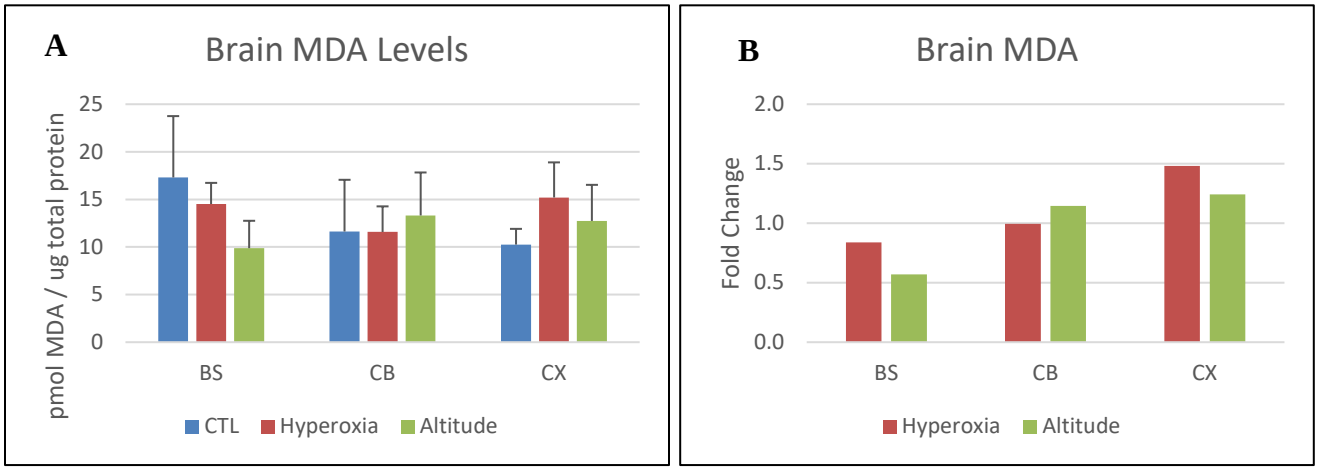

Figure 16. A) Brain tissue levels of MDA. Levels of MDA as a marker of non-specific lipid peroxidation in hyperoxic (HYP) and hypobaric (ALT) conditions relative to control (CTL). CX – cortex; BS – brainstem; CB – cerebellum. Data are mean ± SEM. (n=4-6 for all groups, * p≤0.05 relative to control). B) Fold change in MDA levels relative to control.

Note: BS dataset does not include 72 (CTL), 57 (ALT), or 64 and 65 (HYP).

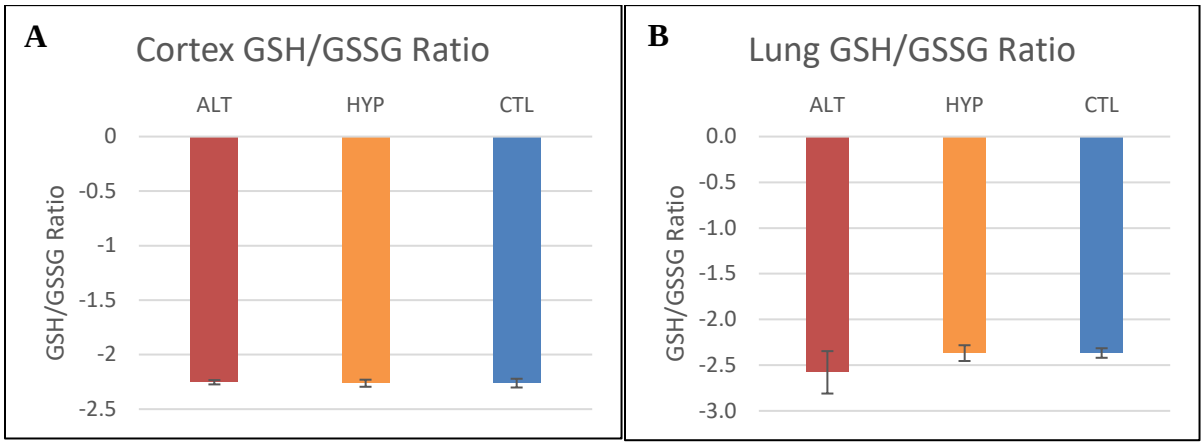

Figure 17. A) Brain cortex and B) Lung ratios of GSH/GSSG as a marker of oxidative stress in hypobaric (ALT) and hyperoxic (HYP) conditions relative to control (CTL). Data are mean ± SEM. (n=4-6 for all groups).

After analyzing six samples within each treatment group with two different staining techniques (H&E staining as well as LBF), it was determined that any histologic changes present were within the normal limits (Table 6). Figure 18 shows a level 4 (midbrain) section of a control sample, stained with both H&E (Figure 18A) and LFB (Figure 18B). As expected, these images show no histologic changes.

4.4 Histopathology Results

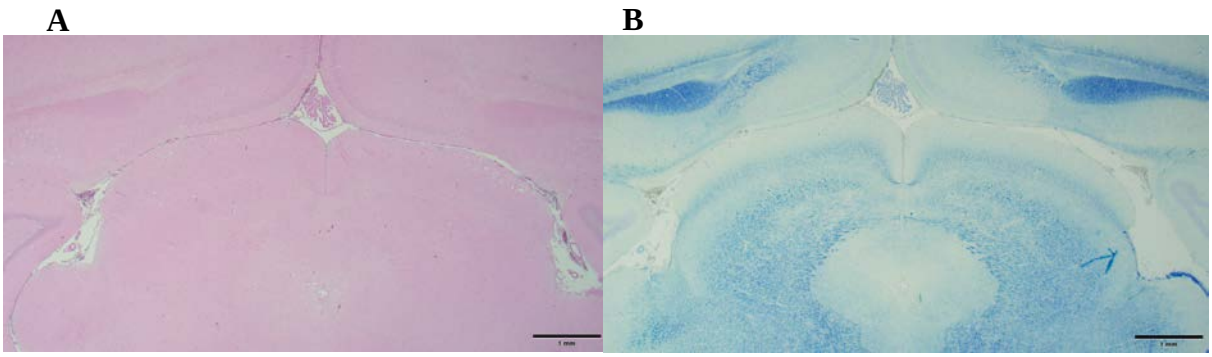

Figure 18. Histopathology results

A) H&E staining of a control sample, level 4, at 2X magnification and B) LFB staining of the same sample, level 4, at 2X magnification.

Table 6. Severity grade of pathologic changes in 18 animal brain samples

Levels are previous described in Figure #, and the grading scale in Table #.

Animal Number	Path Accession #	Treatment Group	H&E Level 2	H&E Level 3	H&E Level 4	H&E Level 6	LFB Level 2	LFB Level 3	LFB Level 4	LFB Level 6
4	19-0252	C1	0	0	0	0	0	0	0	0
6	19-0253	C1	0	0	0	0	0	0	0	0
10	19-0254	C2	0	0	0	0	0	0	0	0
12	19-0255	C2	0	0	0	0	0	0	0	0
16	19-0256	C3	0	0	0	0	0	0	0	0
18	19-0257	C3	0	0	0	0	0	0	0	0
22	19-0258	A1	0	0	0	0	0	0	0	0
24	19-0259	A1	0	0	0	0	0	0	0	0
34	19-0262	A2	0	0	0	0	0	0	0	0
36	19-0263	A2	0	0	0	0	0	0	0	0
46	19-0266	A3	0	0	0	0	0	0	0	0
48	19-0267	A3	0	0	0	0	0	0	0	0
28	19-0260	H1	0	0	0	0	0	0	0	0
30	19-0261	H1	0	0	0	0	0	0	0	0
40	19-0264	H2	0	0	0	0	0	0	0	0
42	19-0265	H2	0	0	0	0	0	0	0	0
52	19-0268	H3	0	0	0	0	0	0	0	0
54	19-0269	H3	0	0	0	0	0	0	0	0

4.5 Electrophysiology Results

Effects of high altitude and hyperoxia exposures on efficacy of synaptic transmission in rat hippocampus

Neurotransmission properties were analyzed by measuring field potentials from the CA1 region when the Schaffer collateral was stimulated by biphasic current pulses of varying intensities (10-100 μA). Stimulation of the Schaffer collateral induced responses mainly from glutamatergic synapses as perfusion with glutamate receptor blockers inhibited all responses. Our evoked field responses contained both population spikes as well as field excitatory postsynaptic potentials (fEPSP). Amplitudes were calculated from population spikes and slopes were calculated from the smaller fEPSP responses. We found that exposures to high altitude (supplemented with 100% O2) and hyperoxia alone (100% O2) resulted in increased input-output function. Amplitudes of evoked responses from ALT and HYP rats were significantly increased compared to evoked

responses from control rats with the HYP group showing the greater effect (Figure 19A). Slope calculation yielded statistical significant effect only in the HYP group (Figure 19B).

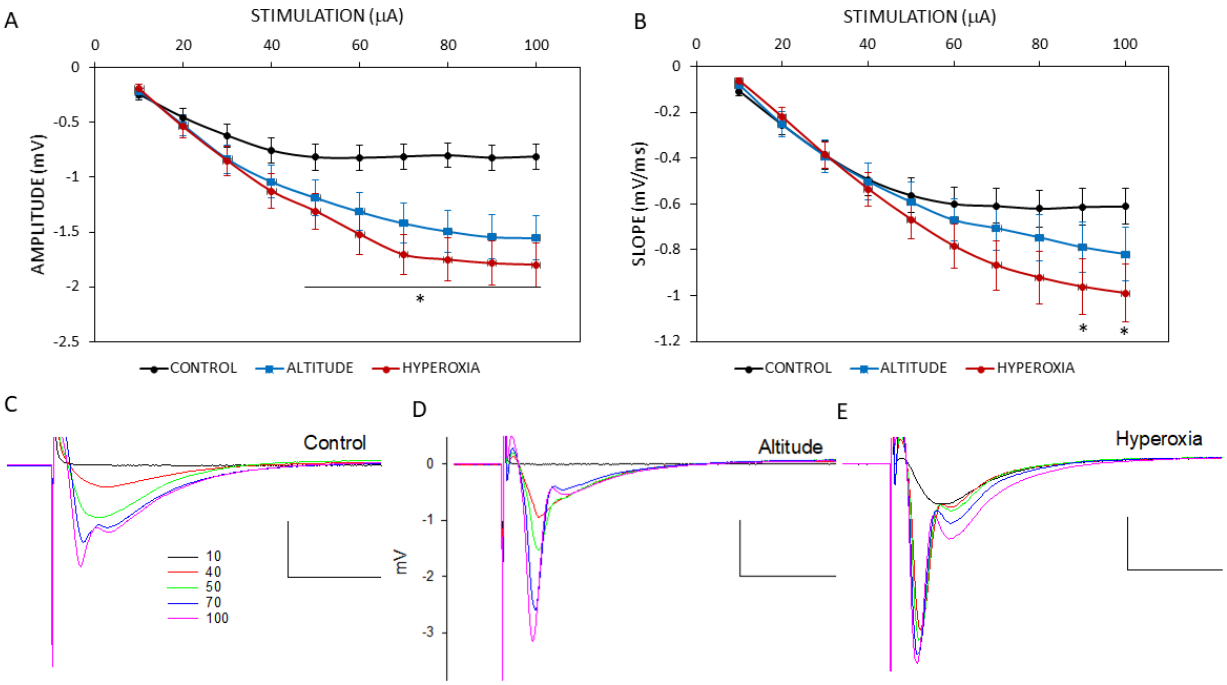

Figure 19. Exposures to high altitude or hyperoxia induced significant increase in input-output response

(A) Input-output relationship graph showing amplitudes of population spikes evoked by 10-100 uA stimulation in the hippocampus from rats exposed to 1000 ft and normal air (control), 30,000 ft and 100% oxygen (altitude) or 1000 ft at 100% oxygen (hyperoxia). Exposures to either high altitude or hyperoxia induced significant increase in evoked responses from hippocampal neurons (P<0.001, two-way ANOVA). Holm Sidak post hoc comparison test revealed significant increases in the range of 60 -100 uA in the altitude group and 50 -100 uA in the hyperoxia group. (B) Input-output relationship graph showing slopes of field potentials evoked by 10-100 uA stimulation in the hippocampus from rats in the control, altitude and hyperoxia groups. Exposures to hyperoxia induced significant increases in the size of evoked responses (P<0.001, two way ANOVA). Holm Sidak post hoc comparison test revealed significant increases in responses when stimulated with 90 and 100 uA . (C-E) Sample input-output voltage traces from control (C), altitude (D) and hyperoxia (E) rats. Scale bars: 1 mV, 10 ms.

Effects of high altitude and hyperoxia exposures on short term synaptic plasticity

Paired pulse facilitation (PPF) is the short term potentiation of response evoked by two consecutive stimuli delivered within tens of milliseconds apart. The belief is that PPF result from the build-up of calcium ions resulting from the paired stimuli delivered very close together. Here, PPF is measured as the ratio of response amplitude or slope from the 2nd stimulus to the response amplitude or slope from the 1st stimulus. The interpulse interval was set to 40 ms. We found that

repetitive exposures to ALT and HYP induced a statistically significant increases in the paired pulse facilitation of hippocampal neurons (Figure 20).

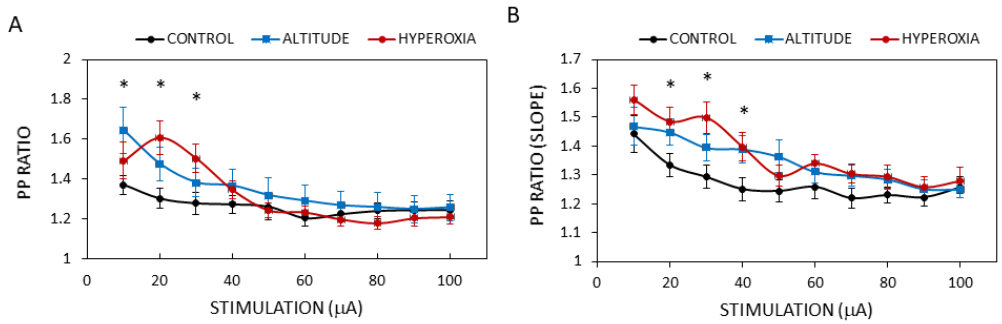

Figure 20. Exposures to high altitude or hyperoxia induced significant increase in paired pulse facilitation (PPF)

(A) Paired pulse ratio (PP Ratio) of amplitudes of population spikes induced by a pair of stimuli (40 ms apart) at various intensities (10-100 uA) was calculated to quantify PPF. Rats exposed to either high altitude (blue) or hyperoxia (red) showed significant increase in PP ratio indicating increased PPF (P=0.002 high altitude vs control, P=0.034 hyperoxia vs control, two way ANOVA). (B) Paired pulse ratio (PP Ratio) calculated from slopes of field potentials induced by a pair of stimuli at various intensities. Rats exposed to either high altitude (blue) or hyperoxia (red) showed significant increase in PP ratio indicating increased PPF (P=0.003 altitude vs control, P<0.001 hyperoxia vs control, two way ANOVA).

Effects of high altitude and hyperoxia exposures on long term synaptic plasticity

We assessed whether exposures to high altitude or hyperoxia can induce lasting changes in long term synaptic plasticity of hippocampal neurons. Long term potentiation (LTP) was induced by a theta burst stimulation (TBS), consisting of 10 repeats of 4 pulses delivered at high frequency (100 Hz). We found that exposures to altitude or hyperoxia did not induce any significant effects on LTP (Figure 21).

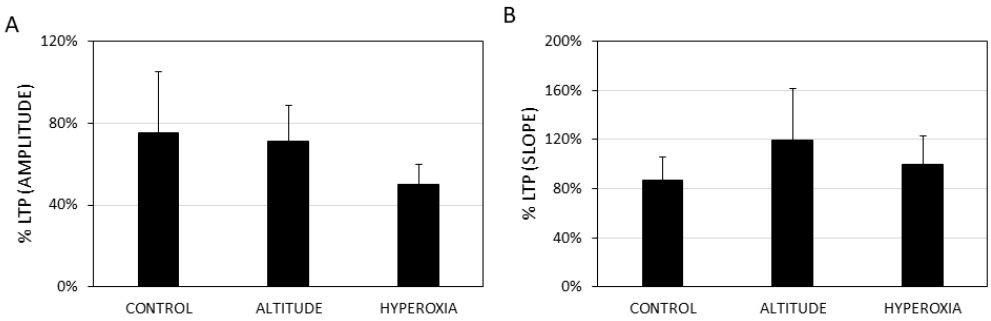

Figure 21. Exposures to high altitude or hyperoxia did not induce significant effects on long term potentiation

(A) Percent potentiation calculated by measuring the amplitudes of population spikes. (B) Percent potentiation calculated by measuring the slopes of field potentials.

Effects of high altitude and hyperoxia exposures on spontaneous activity

Spontaneous activity of hippocampal neurons was recorded over a 10-min period. Spike frequency was calculated and compared across experimental groups. We found that hippocampal

neurons from rats exposed to altitude or hyperoxia had increased frequency in spontaneous spiking activities (Figure 22). One way ANOVA analysis yielded a statistically significant increase in the frequency of spontaneous activity from rats exposed to hyperoxia.

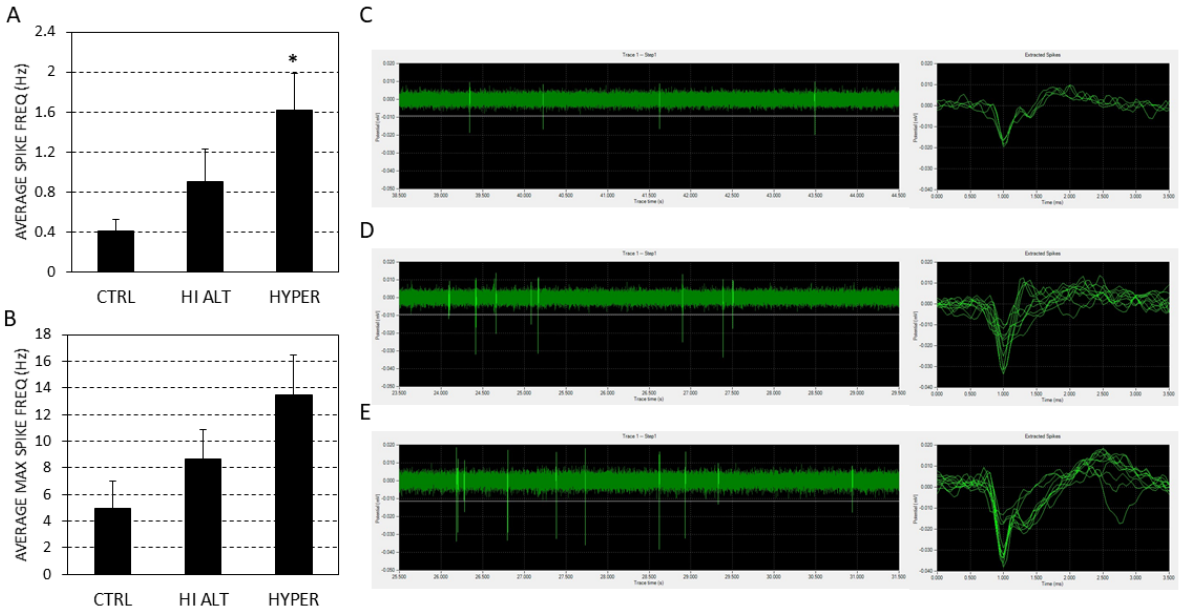

Figure 22. Exposures to high altitude or hyperoxia induced significant increase in spontaneous activity of hippocampal neurons

(A) A bar graph showing the average of the averages of frequency among the different channels within a microelectrode array. Frequencies of spiking activities from each channels from within the microelectrode array of a given slice are calculated and averaged together. Data from multiple slices from the different experimental groups (control, altitude, hyperoxia) are then averaged together. There was a significant increase in the frequency of spontaneous activity from rats exposed to hyperoxia (P=0.022, one way ANOVA). (B) A bar graph showing the average of the maximum frequency among the different channels within a microelectrode array. Frequencies of spiking activities from each channels from within the microelectrode array of a given slice are calculated and the maximum frequency as the spontaneous spiking frequency from that slice. The maximal values from each slice are then averaged together across the different experimental groups. Analysis using t-test suggest significant increase in the averaged maximum frequency (P=0.029) but ANOVA testing yielded P=0.06. (C-E) Sample spontaneous spiking activity data (left) and sample extracted spontaneous spikes (right) from control (C), altitude (D), and hyperoxia (E) rats.

Overall, our data suggest that repeated prolonged exposures to 100% oxygen can result in the hyper-excitability of hippocampal neurons.

5.0 DISCUSSION

This report summarizes the findings of a follow on study investigating the effects of hypobaria and hyperoxia on histopathology, electrophysiology, and cellular and molecular functions in the brain, using a rat model. A multi-disciplined, systems biology approach was used to understand more fully the mechanistic basis of adverse effects caused by exposure to extreme stressors experienced by high altitude pilots, namely hypobaria and hyperoxia. The rat model was chosen to complement the research efforts conducted in mini-pigs by researchers in USAFSAM. Animal to human extrapolation has been recognized as a limitation to animal research and it is recognized that the rat brain is different in size, structure, and vasculature from the human brain and, therefore, not the perfect model for investigating the induction of WMH. However, given the alternative being the use of cellular models, utilizing a fully functioning organism capable of exhibiting full body physiological responses to stressors allows for a robust examination of structural, cellular, and molecular changes to these stressors. The addition in this study of brain histopathology and hippocampal electrophysiology allows for the determination of structural insults and a functional readout. Although WMH have not been induced in rats (or any animals) in response to hypobaria, it is interesting to note is that WMH can be induced in a rat model after an ischemic event (Huang et al., 2010).

The approach undertaken was to examine the effects of hypobaria and hyperoxia at three levels; molecularly, functionally, and structurally. At the molecular level proteomics, metabolomics, and biochemical assays were selected for multiple reasons. Several biochemical assays were performed to examine any induction of stress (corticosterone) or oxidative stress (MDA, that may have resulted due to the exposures. Proteomics was selected because it is a powerful tool that can link altered proteins to discrete signaling pathways, cellular functions and regions of the cell. Lipid NMR-based metabolomics offers critical insight into all lipid species, but more specifically the phospholipids. Because the WMH appear to be localized to the peri-axonal regions, these phospholipids are of particular interest as they define cellular structure, protection and signaling.

Although the number and length of the exposures was doubled from the original preliminary study, the majority of the rats appeared to be fairly tolerant to the exposure conditions. All rats maintained typical behavior patterns, including exploring their new environment, grooming and ultimately sleeping. Interestingly, corticosterone levels in serum were significantly elevated in the ALT group relative to control indicating that despite their outward appearances, they were experiencing stress as a result of the exposures. The serum levels of corticosterone in the HYP group were elevated from CTL, but not statistically significant. The HYP group was included to attempt to separate the effects of high levels of oxygen from the effects caused by hypobaria. However, exposure to 100% oxygen is considered to be potentially toxic. In fact, due to pulmonary and lethality issues in rats, 100% oxygen cannot be administered at sea level for many consecutive hours. To address this, the altitude of the hyperoxic group was elevated to 2500 feet. In addition to general stress, the lipid-rich environment of the brain makes it a vulnerable target for oxidative stress, manifesting as lipid peroxidation. The adverse effects of lipid peroxidation include a decrease in membrane fluidity with a corresponding increase in membrane leakiness, as well as damage to the many membrane proteins, including receptors, transporters, enzymes and ion channels (Halliwell, 2006). Indeed, proteomics results revealed

some distinct and some overlapping proteins and pathways affected by ALT or HYP exposure in the cortex and hippocampus. For example Hpca, a calcium binding protein in the neuronal calcium sensor family, was downregulated in the HYP group of CX. Interestingly, extracellular calcium was shown to play a major role in mediating white matter damage induced by trauma (Stys et al. 1990). Similarly, a glutamate receptor, Gria2, was upregulated in both the ALT and HYP groups in the HC. The HYP group had slightly higher Gria2 expression than the ALT which supports the results seen in the hippocampal neuronal hyperexcitability. Conversely, levels of MDA were not significantly elevated in any of the selected brain regions. Lung was also considered to be a potential target organ for oxygen toxicity, and was therefore assayed for markers of oxidative stress. No changes in oxidized glutathione levels were observed in the lung or cortex of the brain either. Future studies should include a measure of the enzymatic enzymes (catalase, hydrogen peroxidase and superoxide dismutase) as early indicators of a cellular response to oxygen toxicity and oxidative stress. These indices may be more sensitive markers of oxygen toxicity.

Lipid extracts from rat cortex (CX) and cerebellum (CB) samples, including animals from all three experimental groups (CTL, HYP, ALT), display unique metabolite patterns measured by 13C NMR. This analysis is capable of measuring signals from various fatty acids, triacylglycerols, and cholesterol. Principle components analysis (PCA) of these spectral data show separate clusters for CX and CB samples, which are significantly separated in PC-space, as verified by a Davies Bouldin Index value of 0.03. This result is not unexpected as these brain regions are uniquely different in function and would be expected to show slightly different lipid metabolite profiles. More importantly, however, we were unable to find any significant differences between experimental groups: (1) a PCA model for CB samples only shows no separation between CTL, HYP and ALT groups, and (2) a PCA model for CX samples only shows no separation between CTL, HYP and ALT groups. Additionally, the 31P NMR analysis of lipid extracts provided a means to quantify brain phospholipids. We identified 12 specific phospholipid species in these NMR spectra plus 5 unknown peaks, likely belonging to other unidentified phospholipids. We quantified these metabolites relative to tissue weight (μmol/g tissue) and compared the mean values between experimental groups within each tissue type (CB and CX). Some metabolite signals were not observable in all samples; thus, *n*-values are very small for some analyses and their associated error estimates are quite large, precluding any reliable statistics. Albeit, no statistically significant differences were found for any of these phospholipid metabolites between CTL, HYP, and ALT groups. We also expressed each individual phospholipid relative to the total pool size of phosphatidylcholine (one of the most abundant phospholipids in these tissues). Again, there were no statistical differences observed between experimental groups. Taken together, our analyses of brain lipid extracts from rats exposed to hypobaria ± hyperoxia do NOT reveal any differences in lipid metabolites in cerebellum or cortex samples that can be attributed to treatments. Clear differences can be observed between brain regions (cortex *vs.* cerebellum), but these differences do not extend to the experimental treatment groups.

Indeed, proteomics results indicate that regulated proteins seen in the cortex and the hippocampus show some trends for pathway regulation. This was not identified in the brainstem nor the cerebellum. Overall, the proteomics data revealed mild effects of HYP or ALT exposures with less than 2.3% regulated proteins in all four brain regions. In order to see these minimal

changes, a newly optimized proteomics workflow, including label-free samples and a stepwise LC gradient, had to be developed prior to data acquisition (Trudgian et al. 2014). A robust and reliable LC-MS/MS approach is the prerequisite to uncover changes in protein profiles, especially for exposures where only moderate changes are expected, or for proteins with low abundance. A comparison to data obtained using a different protein extraction method or a linear LC gradient revealed that less than half of the total amount of proteins were identified (data not shown). More proteins were changed in the HYP group as compared to the ALT group for all brain regions combined, which indicates that the HYP exposure resulted in a more severe phenotype than ALT exposure. In addition, significant changes in protein abundance were unique between HYP and ALT suggesting distinct molecular effects resulting from each exposure scenario. For example, Hpca was shown to be downregulated in the HYP group of CX, and Gria2 was upregulated in for both treatment groups in the HC. HC showed the highest total number of significantly regulated proteins, which could be partially due to a higher total number of identified proteins. Future work using a more severe exposure protocol will aid in identifying the mechanistic basis of the injury and the brain region that is affected most by hypobaria and/or hyperoxia.

One of the important additions to this study that was not included in the preliminary study was a global examination of brain histopathology. Because the U-2 pilots have shown increased incidence of WMH, we wanted to examine the brains of the animals that had been subjected to repetitive hypobaria and hyperoxia. While we did not expect 2 weeks of exposures to cause the level of damage to induce a WMH, we did hypothesize that repetitive insults might lead to a modest level of structural damage or changes to the brain integrity in the study animals. H&E staining and luxol fast blue staining was performed on serially dissected brains which included almost every major landmark (Levels 2, 3, 4 and 6 - see Table 1). H&E staining was performed to examine overall brain structural integrity. Luxol fast blue staining was included because it stains myelin and can be used to determine damage to myelination in the brain, something thought to happen in brain regions where WMH are observed. No regions showed any structural issues and it was determined that any histologic changes present were within the normal limits.

The inclusion of hippocampal electrophysiology was another important addition to the current study that was lacking in the preliminary study. In addition to brain structure, the electrophysiological effects of high altitude and hyperoxia on the hippocampus could be critical to airman mission. The hippocampus is critical for the learning process as well as memory function and has been implicated in other cognitive functions. Investigating the effects on the general integrity of synaptic transmission might yield insight into neuron excitability. Previously, increases in the input-output responses of hippocampal neurons have been correlated with apnea-induced glutamate excitotoxicity that can subsequently induce neuronal apoptosis (Fung et al., 2012) as well as with hyperexcitability resulting from pilocarpine-induced acute seizures (Amakhin et al., 2017). Both the ALT and HYP groups showed significant increases in evoked responses compared to the control. Interestingly, the HYP group showed the greatest increase. This might be due to the altitude lowering the actual oxygen exposure in the ALT group. The effects of ALT and HYP on short term synaptic plasticity were also investigated and both the ALT and HYP groups showed statistically significant increases in the paired pulse facilitation. An increase in PPF that is accompanied by a reduction in the input-output response typically means that there is a reduction in the probability of neurotransmitter release. However,

we do not think that the observed increase in PPF resulted from decreased probability in the neurotransmitter release because we also observed a significant increase in our input-output function. We believe the increase in PPF is more likely to result from an increase in neuronal excitability since PPF increase has also been correlated with hyper-excitability in an animal model of epilepsy (Wu and Leung 2003). Long term synaptic plasticity (LTP) was also examined in the hippocampus. Exposure to ALT or HYP did not induce significant effects on LTP. Additionally, spontaneous activity of hippocampal neurons was measured. It was observed that hippocampal neurons displayed greater frequency of spontaneous spiking activity following prolonged exposures to hyperoxia (HYP), which is also consistent with the hypothesis that the exposures induced an increased excitability of CA1 hippocampal neurons

This study successfully examined the effects of hypobaria and hyperoxia using a rodent model. Preliminary studies indicated that the altitude chamber could capably generate extreme levels of hypobaria and also deliver 100% oxygen. The rats were tolerant of the exposures in both the preliminary and present studies. While structural changes were not observed, once again, molecular and functional changes were measurable. Low levels of stress were evident as well as proteomic changes in the hippocampus and cortex of the brain. Importantly, hippocampal neurons presented hyper-excitability in response to both ALT and HYP exposures. The inclusion of molecular and functional changes combined with the lack of structural damage could lead one to multiple conclusions: 1) We are not exposing the rats long enough or often enough to induce structural insults to the brain; 2) Rats (rat brains) are not a good model for studying hypobaria and/or hyperoxia; 3) We possibly need to examine the brains at a much higher magnification (TEM) to detect myelination issues; etc. While hypobaria has not been utilized successfully to induce WMH in an animal model yet, it is known that WMH can be induced in a rat model after an ischemic event (Huang et al., 2010). Given the convincing human MRI data on U-2 pilots, it stands to reason that years of prolonged hypobaric exposure probably leads to increases in WMH in people. Whether it is worth it to run a chronic hypobaric animal study to finally induce WMH in an animal model remains to be seen. Ultimately, the goal was to increase exposure frequency and duration with the hopes of seeing cellular and molecular changes that might be indicative of a pre-structural insult. To that end, the study was a success as both proteomic and electrophysiological measures showed significant changes from the control. The proteomics and electrophysiology indicate that subclinical changes are occurring even though they have not resulted in biochemical or structural changes detectable by NMR, stress endpoints or histopathology; again suggesting a chronic animal study. The potential payoff is the knowledge gained from this study can be used in designing new studies and helping with approaches to mitigate operational risks and long-term adverse health outcomes associated with high-altitude flight.

6.0 REFERENCES

Amakhin DV, Malkin SL, Ergina JL, Kryukov KA, Veniaminova EA, Zubareva OE, Zaitsev AV. 2017. Alterations in properties of glutamatergic transmission in the temporal cortex and hippocampus following pilocarpine induced acute seizures in Wistar rats. Frontiers in Cellular Neuroscience. 11:264.

Anderson, P.E., Mahle, D.A., Doom, T.E., Reo, N.V., DelRaso, N.J., Raymer, M.L. 2010. Dynamic adaptive binning: an improved quantification technique for NMR spectroscopic data. Metabolomics. 7:179-190.
Forgacs, A.L., Kent, M.N., Makley, M.K., Mets, B., DelRaso, N., Jahns, G.L., Burgoon, L.D., Zacharewski, T.R. and Reo, N.V. 2012. Comparative metabolomic and genomic analyses of TCDD-elicited metabolic disruption in mouse and rat liver. Toxicol Sci. 125(1): 41-55.

Fung, S.J., Xi, M.C., Zhang, J.H., Sampogna, S., Chase, M.H. 2012. Apnea produces excitotoxic hippocampal synapses and neuronal apoptosis. Experimental Neurology. 238: 107-113.

Halliday, K.R, Fenoglio-Preiser, C. and Sillerud, L.O. 1988. Differentiation of human tumors from nonmalignant tissue by natural-abundance ^{13}C NMR spectroscopy. Magn Reson Med. 7: 384-411.

Halliwell, B. 2006. Oxidative stress and neurodegeneration: Where are we now? J Neurochem. 97: 1634-58.

Huang, Y., Zhang, W., Lin, L, Feng, J, Chen, F., Wei, W., Zhao, X., Guo, W., Li, J., Yin, W. and Li, L. 2010. Is endothelial dysfunction of cerebral small vessel responsible for white matter lesions after chronic hypoperfusion in rats? J Neurol Sciences. 299:72-80.

McGuire, S., Sherman, P., Profenna, L., Grogan, P., Sladky, J., Brown, A., Robinson, A., Rowland, L., Hong, E., Patel, B., Tate, D., Kawano, E.S., Fox, P. and Kochunov, P. 2013. White matter hyperintensities on MRI in high altitude U-2 pilots. Neurology. 81(8):729-35.

McGuire, S.A., Sherman, P.M., Brown, A.C., Robinson, A.Y., Tate, D.F., Fox, P.T. and Kochunov, P.V. 2012. Hyperintense white matter lesions in 50 high-altitude pilots with neurologic decompression sickness. Aviat Space Environ Med. 83(12):1117-1122.

McGuire, S.A., Tate, D.F., Wood, J., Sladky, J.H., McDonald, K., Sherman, P.M., Kawano, E.S., Rowland, L.M., Patel, B., Wright, S.N., Hong, E., Rasmussen, J., Willis, A.M. and Kochunov P.V. 2014. Lower neurocognitive function in U-2 pilots: Relationship to white matter hyperintensities. Neurology. 83(7): 638-45

Meneses, P. and Glonck, T. 1988. High Resolution ^{31}P NMR of extracted phospholipids. J Lipid Res. 29: 679-689.

Rao, D. B., Little, P. B., Malarkey, D. E., Herbert, R. A., and Sills, R. C. (2011). Histopathological evaluation of the nervous system in National Toxicology Program rodent studies: A modified approach. Toxicol Pathol 39, 463–70.

Sillerud, L.O., Han, C.H., Bitensky, M.W. and Francendese, A.A. 1986. Metabolism and structure of triacylglycerols in rat epididymal fat pad adipocytes determined by ^{13}C nuclear magnetic resonance. J Biol Chem. 261: 4380-8.

Stys, P.K., Ransom, B.R, Waxman, S.G. and Davis, P.K. 1990. Role of extracellular calcium in anoxic injury of mammalian central white matter. Proc Natl Acad Sci U S A. 87(11): 4212-6.

Tyagi, R.K., Azrad, A., Degani, H. and Salomon, Y. 1996. Simultaneous extraction of cellular lipids and water-soluble metabolites: evaluation by NMR spectroscopy. Magnet Reson Med. 35: 194-200.

Trudgian, D. C., Fischer, R., Guo, X., Kessler, B. M., & Mirzaei, H. 2014. GOAT--a simple LC-MS/MS gradient optimization tool. Proteomics, 14(12): 1467–1471.

Tyanova, S, Temu, T., Sinitcyn, P., Carlson, A., Hein, M.Y., Geiger, T., Mann, M. and Cox, J. 2016. The Perseus computational platform for comprehensive analysis of (prote)omics data. Nature Methods. 13: 731–740.

Tyanova, S., Temu, T. and Cox, J. 2016. The MaxQuant computational platform for mass spectrometry-based shotgun proteomics. Nature Protocols. 11: 2301–2319.

Wu, K and Leung, LS. 2003. Increased dendritic excitability in hippocampal CA1 in vivo in the kainic acid model of temporal lobe epilepsy: a study using current source density analysis. Neuroscience. 116: 599-616.

LIST OF ACRONYMS

^{13}C	Carbon 13
^{1}H	Proton
^{31}P	Phosphorous 31
8-isoP	8-Isoprostane
AGC	Automatic Gain Control
ALT	Altitude
BS	Brainstem
CB	Cerebellum
$CDCl_3$	Deuterated chloroform
cDNA	Complementary deoxyribonucleic acid
$CHCl_3$	Chloroform
CID	Collusion-Induced dissociation
CRP	C reactive protein
Cs_2(EDTA)	Cesium ethylene diamine tetraacetic acid
CTL	Control
CX	Cortex
D_2O	Deuterated water
DCS	Decompression sickness
ddH_2O	Double distilled water
dNTP	Deoxynucleotide triphosphate
ELISA	Enzyme linked immunosorbent assay
FA	Fatty acid
GSH	Glutathione
GSSG	Oxidized glutathione
HP	Hippocampus
HPLC	High performance liquid chromatography
HYP	Hyperoxia
Hz	Hertz
Ifn-γ	Interferon gamma
Il-6	Interleukin 6
kHz	Kilohertz
LC	Liquid chromatography
LC-MS/MS	Liquid chromatography tandem mass spectrometry
MDA	Malondialdehyde
MeOH	Methanol
MHz	Megahertz
MRI	Magnetic resonance imaging
mRNA	Messenger ribonucleic acid
NDCS	Neurological decompression sickness
Nfκb	Nuclear factor kappa B
NMR	Nuclear magnetic resonance
NOE	Nuclear Overhauser Enhancement

OPLS-DA	Orthogonal Projections onto Latent Surfaces Discriminant Analysis
PCA	Principal component analysis
PCR	Polymerase chain reaction
PUFA	Polyunsaturated fatty acid
RIA	Radioimmunoassay
RNA	Ribonucleic acid
rpm	Revolutions per minute
RT	Reverse transcription
SCX	Strong cation exchange
SD	Sprague Dawley
SEM	Standard error of the mean
TMS	Trimethylsilane
TMT	Tandem mass tags
Tnf-α	Tumor necrosis factor alpha
TPP	Triphenyl phosphate
TSP	2, 2`, 3, 3`-deuterotrimethylsilylpropionic acid
USAFSAM	United States Air Force School of Aerospace Medicine
WMH	White matter hyperintensity